AD-A073 361 NAVAL POSTGRADUATE SCHOOL MONTEREY CA F/G 17/5
EXPERIMENTAL FLIR STUDY.(U)
JUN 79 J P GRUBER

UNCLASSIFIED

| OF |
AD A073361

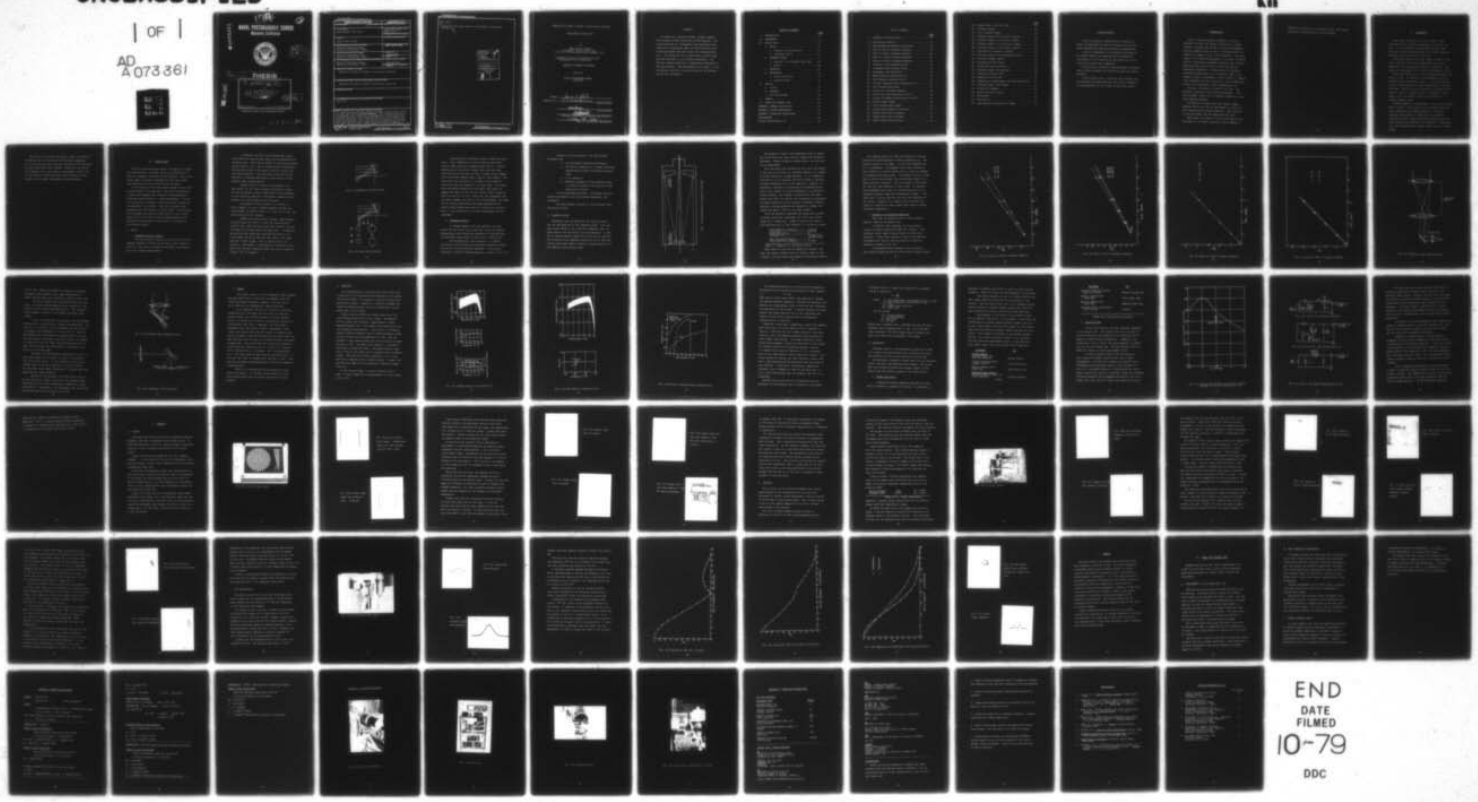

END
DATE FILMED
10-79
DDC

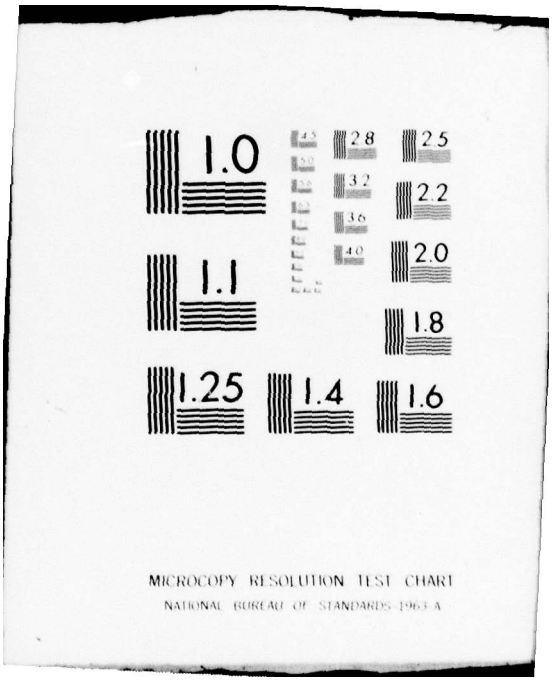
1.0
1.1
1.25
1.4
1.6
2.0
2.2
2.5
2.8
3.2
3.6
4.0
MICROCOPY RESOLUTION TEST CHART
NATIONAL BUREAU OF STANDARDS 1963-A

(2)

NAVAL POSTGRADUATE SCHOOL

Monterey, California

(9) Master's THESIS

(6) EXPERIMENTAL FLIR STUDY.

by

(10) James Powell/Gruber

(11) Jun[redacted]79

(12) 80p.

Thesis Advisor: E. C. Crittenden Jr.

Unclassified

SECURITY CLASSIFICATION OF THIS PAGE (When Data Entered)

REPORT DOCUMENTATION PAGE		READ INSTRUCTIONS BEFORE COMPLETING FORM
1. REPORT NUMBER	2. GOVT ACCESSION NO.	3. RECIPIENT'S CATALOG NUMBER
4. TITLE (and Subtitle) Experimental FLIR Study		5. TYPE OF REPORT & PERIOD COVERED Master's Thesis; June, 1979
		6. PERFORMING ORG. REPORT NUMBER
7. AUTHOR(s) James Powell Gruber		8. CONTRACT OR GRANT NUMBER(s)
9. PERFORMING ORGANIZATION NAME AND ADDRESS Naval Postgraduate School Monterey, California 93940		10. PROGRAM ELEMENT, PROJECT, TASK AREA & WORK UNIT NUMBERS
11. CONTROLLING OFFICE NAME AND ADDRESS Naval Postgraduate School Monterey, California 93940		12. REPORT DATE June, 1979
		13. NUMBER OF PAGES 79
14. MONITORING AGENCY NAME & ADDRESS(if different from Controlling Office) Naval Postgraduate School Monterey, California 93940		15. SECURITY CLASS. (of this report) Unclassified
		15a. DECLASSIFICATION/DOWNGRADING SCHEDULE

16. DISTRIBUTION STATEMENT (of this Report)

Approved for public release; distribution unlimited

17. DISTRIBUTION STATEMENT (of the abstract entered in Block 20, if different from Report)

Approved for public release; distribution unlimited

18. SUPPLEMENTARY NOTES

19. KEY WORDS (Continue on reverse side if necessary and identify by block number)

NPS FLIR

20. ABSTRACT (Continue on reverse side if necessary and identify by block number)

A single cell, serially scanned, thermal imaging FLIR system has been constructed ~~at NPS Monterey~~. The system consisted of a Cassegrain type reflecting telescope with a convergent beam, oscillating mirror scan system and HgCdTe and InSb single cell infrared detectors. The system was first tested using visible light and then switched to the infrared wavelengths. The FLIR has imaged scenes with a temperature difference of 9°K above ambient. MTF measurements have shown it to be diffraction-

DD FORM 1 JAN 73 1473 (Page 1)

EDITION OF 1 NOV 65 IS OBSOLETE

S/N 0102-014-6601 |

Unclassified

SECURITY CLASSIFICATION OF THIS PAGE (When Data Entered)

20. cont.:

limited by the active area of the detector crystal and the optics.

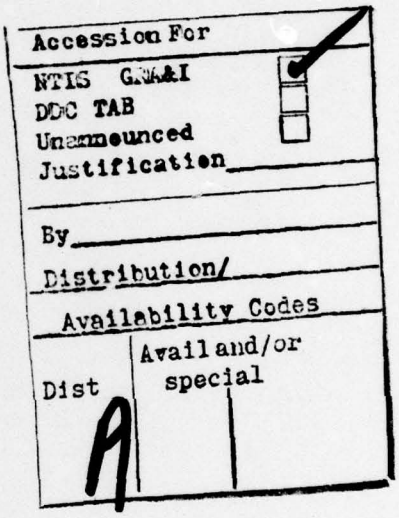

Approved for public release; distribution unlimited

Experimental FLIR Study

by

James Powell Gruber
Lieutenant, United States Navy
B.S.S.E., United States Naval Academy, 1973

Submitted in partial fulfillment of the
requirement for the degree of

MASTER OF SCIENCE IN PHYSICS

from the

NAVAL POSTGRADUATE SCHOOL
June, 1979

Author James P. Gruber

Approved by: E. A. Crittenden, Jr.
Thesis Advisor

A. W. Cooper
Second Reader

Chairman, Department of Physics and Chemistry

William M. Tolles
Dean of Science and Engineering

ABSTRACT

A single cell, serially scanned, thermal imaging FLIR system has been constructed at NPS Monterey. The system consisted of a Cassegrain type reflecting telescope with a convergent beam, oscillating mirror scan system, and HgCdTe and InSb single cell infrared detectors. The system was first tested using visible light and then switched to the infrared wavelengths. The FLIR has imaged scenes with a temperature difference of $9^{o}K$ above ambient. MTF measurements have shown it to be diffraction limited by the active area of the detector crystal and the optics.

TABLE OF CONTENTS

LIST OF FIGURES

ACKNOWLEDGEMENT

I wish to express my appreciation to Professors Milne and Rodenback for their assistance with the computer programs and detector electronics respectively.

I wish to acknowledge the invaluable assistance of Mr. Robert Moeller who manufactured the mechanical structures of the system and Mr. Ken Smith for his advice on the electronics components.

I would like to specially thank Professor Crittenden whose wisdom, guidance and inspiration made this thesis possible.

I would finally like to thank my wife, Roseann, for her patience and understanding; they were as important to the completion of this thesis as any other factor.

I. INTRODUCTION

FLIR, or Forward Looking InfraRed, is a device designed to detect the thermal differences in remote objects, utilizing that portion of the electromagnetic spectrum commonly known as heat, displaying these differences as images visible to the human eye. The advantages of the infrared wavelengths lie in their increased ability to penetrate atmospheric aerosols and to detect emissions from objects above or below the ambient background temperature. Since man and his machines constantly produce heat as a by-product, night is no longer a cloak of concealment. Other sources of temperature difference also act as sources, such as differences in past sun illumination, water temperatures, etc.

The basic idea behind the FLIR is not new. The earliest system was a circa-1930 Evaporagraph. This was extremely limited due to inherent insensitivity and time response problems.

The ability to create real time thermal images, however, had to wait for the development of sensitive, fast response-time infrared detectors. This occurred in the late 1950's and the modern FLIR was born.

Since then, the advance of solid state physics and the advent of tri-metal detectors, such as HgCdTe or

SnPbTe which require less extreme cooling, have further stimulated the application of these devices.

II. BACKGROUND

Since their inception in the late 1950's, FLIRs have gained ever increasing acceptance in military circles. It is, therefore, increasingly important that military officers become familiar with design, operating principles and limitations of the FLIR.

While FLIR concepts have been taught at NPS for many years, there has been little opportunity for direct experience with the hardware behind the concepts. This thesis was undertaken as a system for experimental study.

There are several uses to which an operating FLIR can be put at NPS. In addition to the knowledge gained by designing and constructing a FLIR, it can be a stepping stone to understanding the newer technologies of present day FLIRS. Several projects utilizing the infrared wavelengths, such as a recent project in atmospheric turbulence, could also benefit from the availability of a thermal imaging system.

Thermal imaging is accomplished, in a FLIR, as follows. Optics collect, filter and focus the infrared radiation from a scene onto an infrared detector. An optical scanning system moves the image across the detector creating a train of analog electrical signals which are then processed and amplified for display on a video monitor; thus converting the infrared scene into its visible analog.

The design of this FLIR was kept as simple as possible to permit study of the effects of individual components and to utilize those parts already available at NPS Monterey. No other constraints were imposed. Preferably the system would operate over a wide band of wavelengths, exhibit all or most facets of FLIR principles and be capable of modification as the newer technologies become available.

III. DESIGN STEPS

The first and overriding concern throughout the design and construction of the FLIR system was optimization in terms of components available at NPS Monterey. Due to the broad range of research undertaken at NPS, parts which were adaptable to FLIR use were easily obtained.

It was decided to work the design through first in the visible region of the spectrum. This eased the problems of focus and alignment and allowed an understanding of subsystem interrelations vs. system performance. The initial design had a catoptric front-end optical system with a catadioptric scan system. With the IR lenses being germanium and thus opaque to visible light, it was thought that designing and setting up the system in the visible region first would allow a better understanding of the principles and problems of FLIRs prior to switching to the infrared region.

A. OPTICS

1. Parabolic Off-Axis Mirror

The first optical design was the use of an 8.57 cm diameter parabolic off-axis mirror with a focal length of 25.87 cm. This type of mirror was available from earlier use in an infrared spectrometer.

A parabolic off-axis mirror experiences severe distortions for arriving rays which are not parallel with the optic axis. This has the effect of limiting the total system field of view. Due to scanner mirror constraints, the limiting effect of the mirror field of view was not considered important. The constraint which led to this decision is discussed more fully in the section on the parallel beam scanning system.

Another factor in favor of the parabolic off-axis mirror was its lack of central obscuration, which allowed the mirror's total surface area to be considered as the collecting aperture. This means a smaller optics package for a given energy collecting area.

A parabolic off-axis mirror is, in effect, a mirror segment cut from a larger parabolic surface and then mounted, as shown in FIG. (1). Prior to its use, the focal point had to be located.

A HeNe laser beam was run through a beam expander and positioned such that it filled the entire mirror. Theoretically, when the focal point was correctly located the image of the beam would be a small spot. In addition, moving the focal plane away from the focal point, in a line between the mirror and the focal point, will cause the spot to grow larger. This is shown in FIG. (2) column a. Any errors in the location of the mirror focal point will manifest themselves when the circle becomes an elipse, FIG. (2) column b.

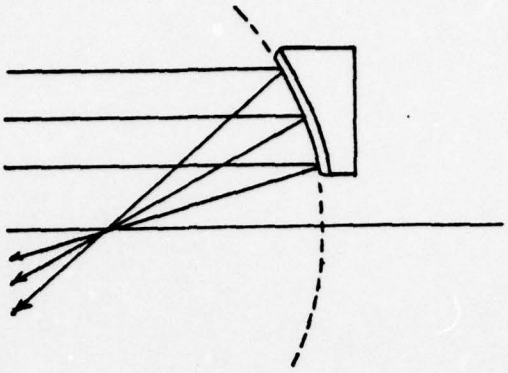

FIG. (1) Parabolic Off-Axis mirror

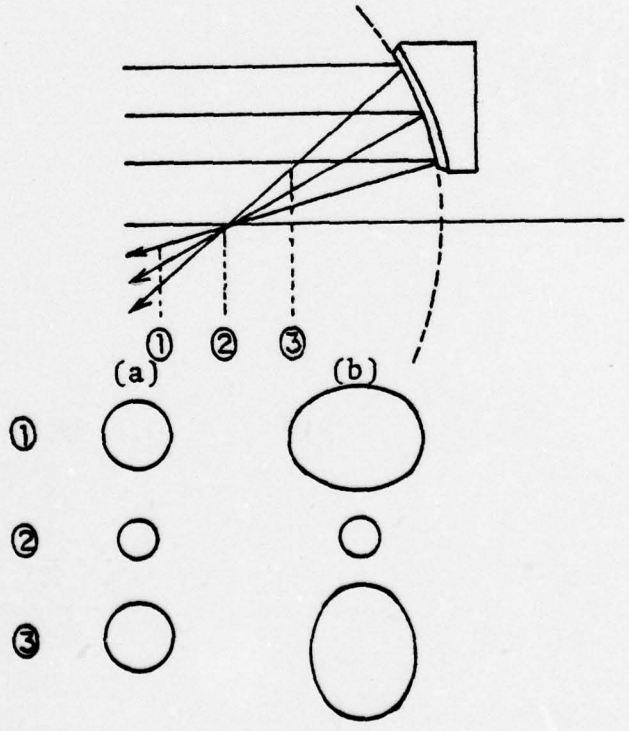

FIG. (2) Focal Point Location

Utilizing this technique quickly located the focal point. Upon attempting to form an image at that point, serious image coma and astigmatism were noted. A closer examination of the mirror brought forth the fact that since the mirror had been cut from a larger mirror segment, the f/# was much smaller than it had at first seemed. The focal point was located 2.54 cm below a line normal to the mirror face and tangent to its lower edge. This means that the minimum diameter of the mirror from which the segment had been cut was 22.2 cm. With a focal length of 25.87 cm, the f/# is 1.16. While this was acceptable when the mirror segment was used in an IR Spectrograph, the small f/# was causing aberrations and image degradation for objects being viewed which were not directly on the optic axis. It was decided to try a more conventional optical telescope.

2. Cassegrain Optics

It became apparent that the parabolic off-axis mirror was not suited to the task and a 15.24 cm diameter Cassegrainian type reflecting astronomical telescope with an equivalent focal length of 228.6 cm was substituted.

The Cassegrainian type telescope is a central obscuration type utilizing an adjustable spherical primary mirror and a fixed elipsoidal secondary. This type of telescope is called a Dahl-Kirkham and is shown in FIG. (3).

Several of the advantages of the Dahl-Kirkham telescope are:

a. It was already assembled and aligned.

b. The 15.24 cm aperture is a large collecting surface which offsets the central obscuration.

c. It is catoptric.

d. Mounting hardware for the scanning system is already attached in the form of an eyepiece screw fitting.

Its disadvantages are minor. The larger size and central obscuration, not being design parameters, are acceptable.

The Dahl-Kirkham telescope is the finalized front end optical system.

B. SCANNING SYSTEM

Concurrent with the design of the front-end optics was the consideration of the scanning system. Since the scan system design is not critically dependent upon the input optics, the two efforts ran simultaneously. A number of options present themselves at this point; however, any decision on the scanning system also has to take into account such other areas as display, image recognition vs. the human eye and detector types.

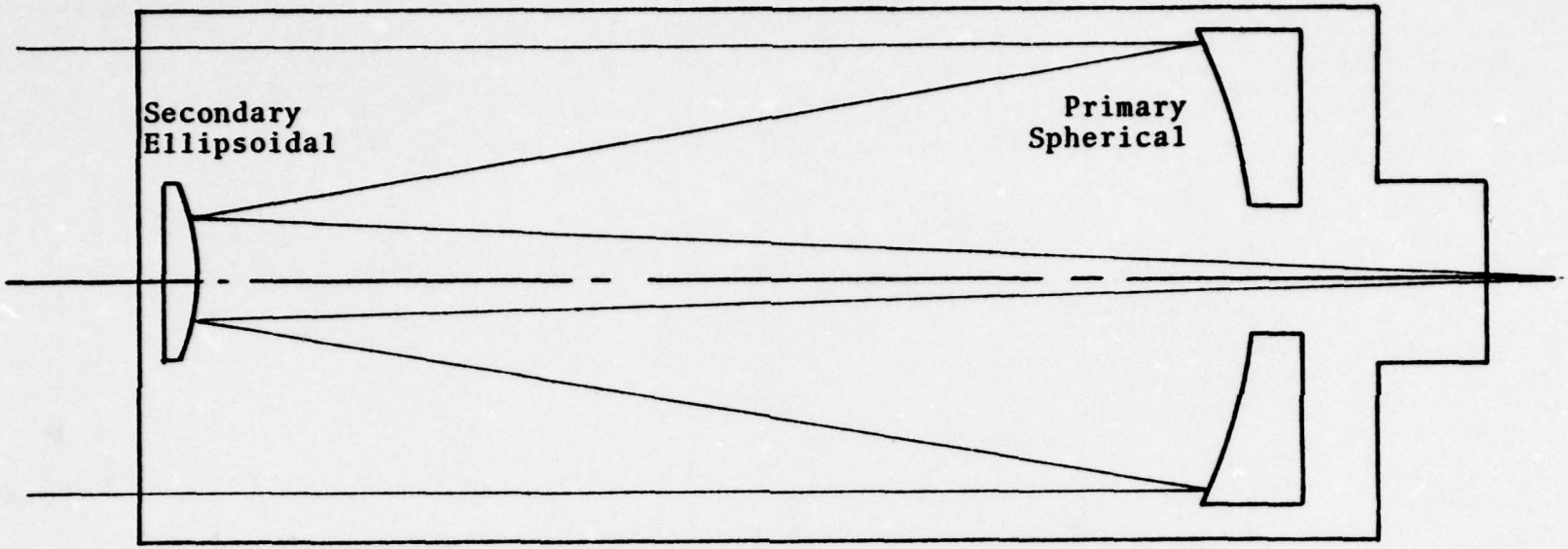

FIG. (3) Dahl-Kirkham Astronomical Telescope

The detector's input to the scanning system is simple due to the fact that there are only single cell detectors available. Without linear or planar arrays, the scan must be two dimensional.

With any device the ultimate use will drive the design. In the case of the FLIR, its ultimate purpose is to present a visible picture to a human operator. It is, therefore, desirable to try to optimize the FLIR display in relation to known characteristics of the human eye. Chapter 4 of Reference 1 contains an interesting and thorough discussion of the subject of visual psychophysics as related to screen viewing. Any attempt to optimize for the human factor must take into account the information so presented. The human interface was not normally considered; however, wherever a design parameter was amenable to change, the change was made in favor of the human element.

Given the amount of knowledge and experience resident in modern television technology, the ideal scan system should be TV compatible. TABLE (I) below lists some of the characteristics of the standard U.S. television raster.

Line Repetition Frequency -------	15750 Hz
Frame Rate ----------	1/30 Sec
Interlaced Fields ----------	Yes
Blanking Time ----------	10 uSec/Line 1000uSec/Frame
Line Utilization Factor ---------	.7
Total Resolution Elements -------	147,000

TABLE (I) Standard U.S. Television Raster

Many FLIRs of today are TV compatible; however, the high scan speeds required rule out several types of scan systems, including those that depend on oscillating mirrors.

The scanning devices on hand are several oscillating plane mirrors manufactured by General Scanning, Inc. The mirrors consist of two types: (i) position feedback and (ii) nonfeedback. The feedback type mirror returns an error signal to a control device which is used to increase or decrease drive motor power. The feedback mirror is then able to follow an arbitrary (non sinusoidal) signal to a high (relative) frequency. This fact makes it the choice for the fast scan dimension of the system. In contrast, the nonfeedback type mirror is limited much more in its frequency response range for nonsinusoidal signals. This means that it can be used for the slow scan dimension of the system. Figures (4-7) contain plots of mirror response as a function of input signal amplitude for various sinusoidal frequencies.

1. Parallel vs. Convergent Beam Scan

There are two general types of scan technique, parallel beam and convergent beam.

In parallel beam scanning, the scan system is located in a region where the images are "afocal." This technique avoids image blurring caused by focal point shifting. A field lens located in front of the detector intercepts the "afocal" beam and focuses it upon the detector as shown in FIG. (8).

In convergent beam scanning, the scan mirrors are located between the optics and the focal plane as shown

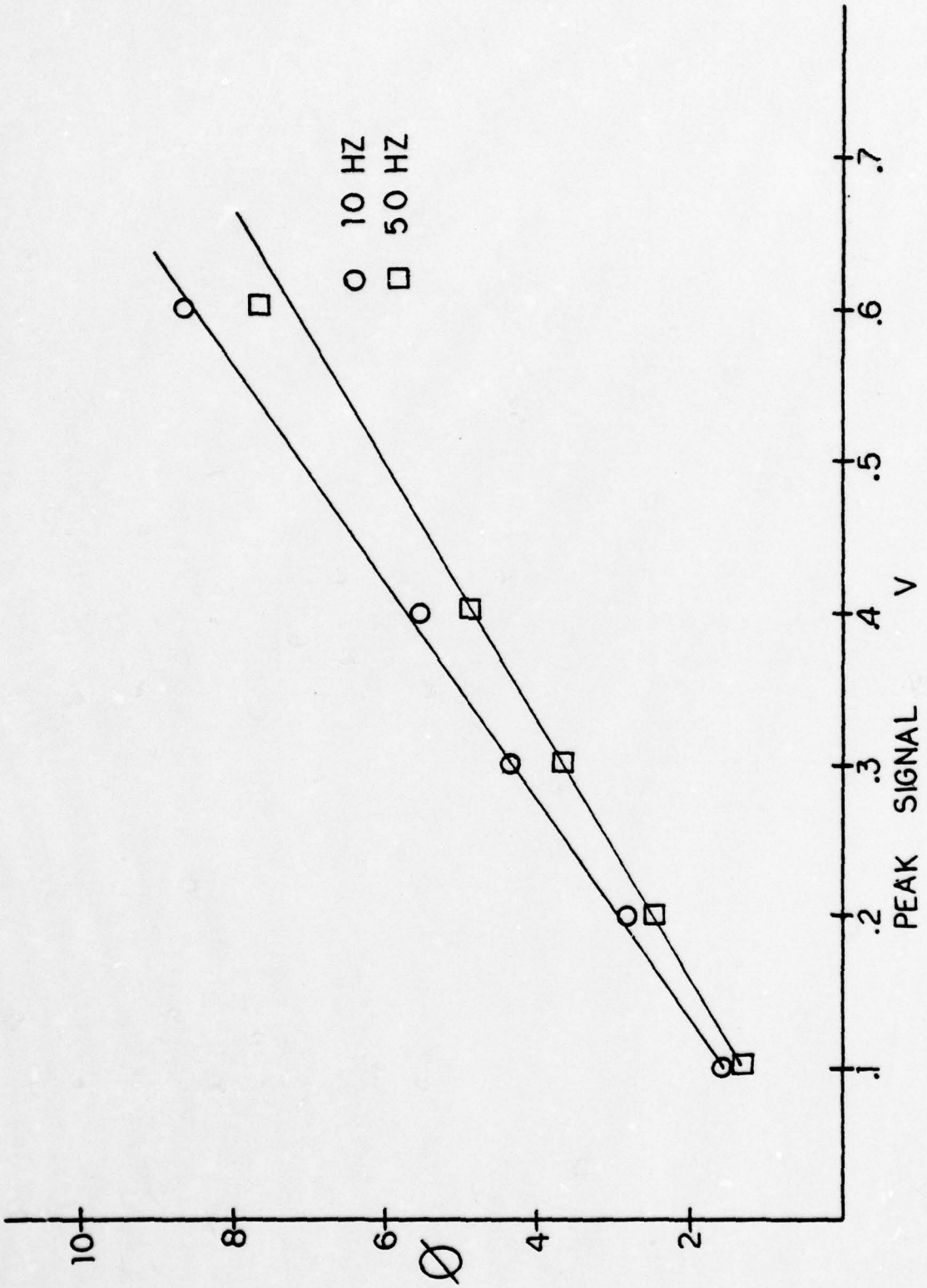

FIG. (4) Type (i) Mirror Frequency Response

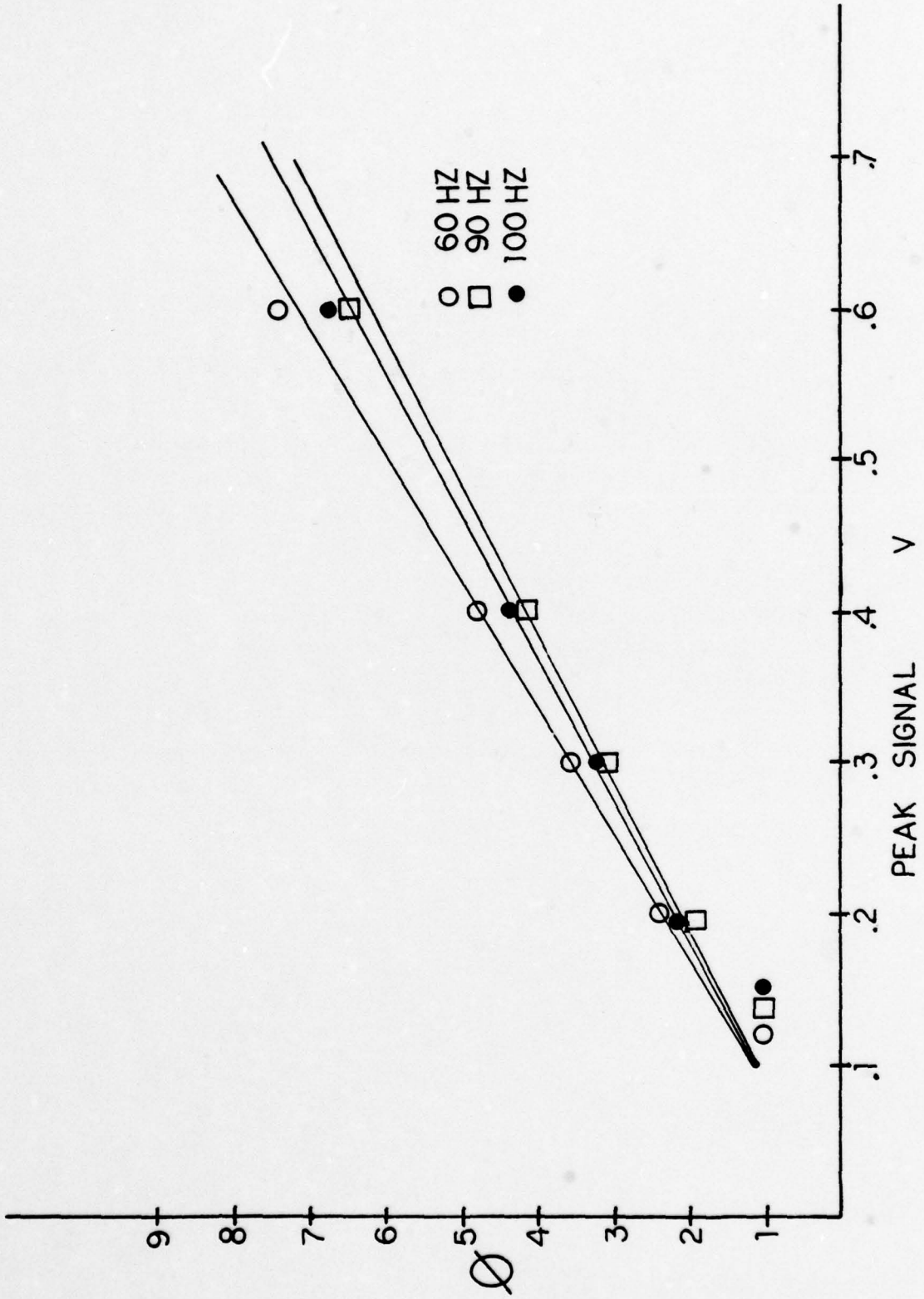

FIG. (5) Type (i) Mirror Frequency Response

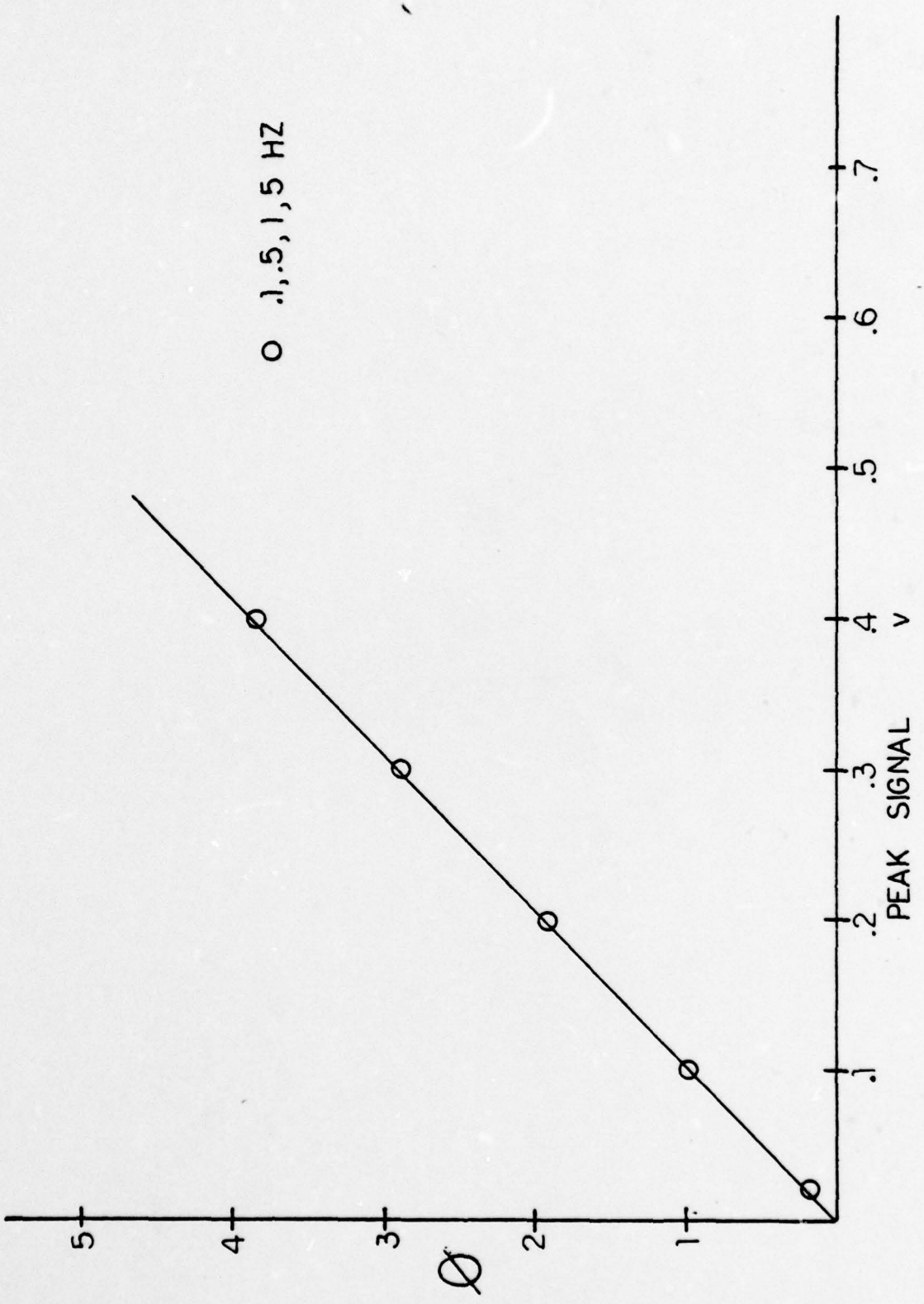

FIG. (6) Type (ii) Mirror Frequency Response

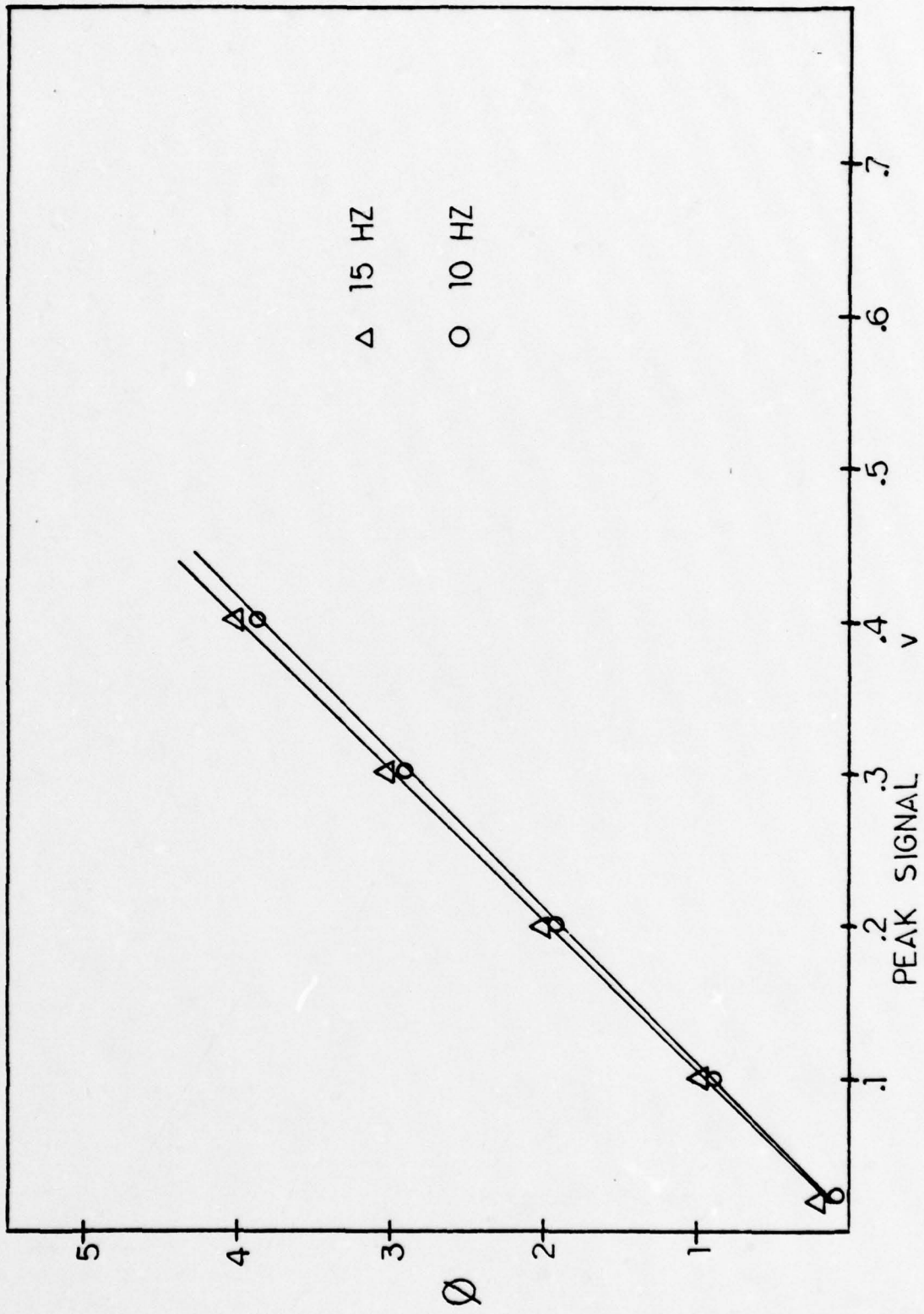

FIG. (7) Type (ii) Mirror Frequency Response

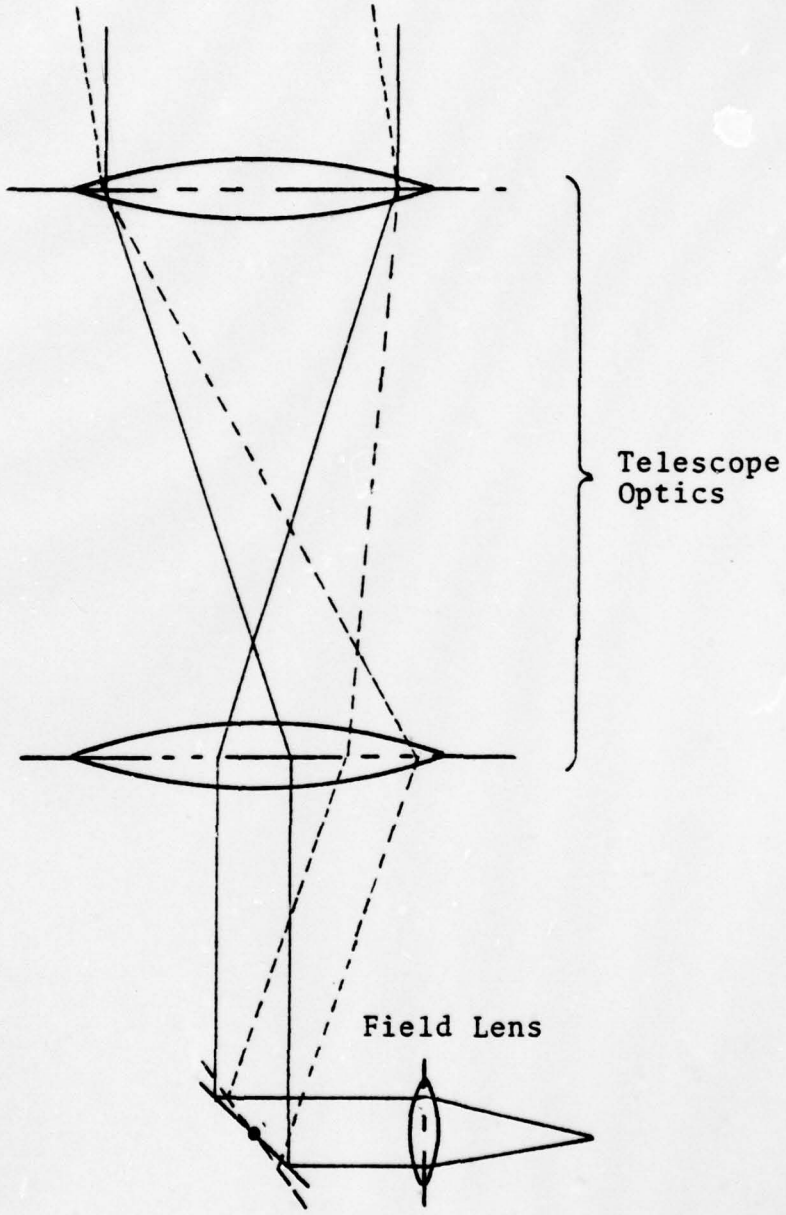

FIG. (8) "Parallel" Beam Scanning System

in FIG. (9). While much simpler to construct and align, convergent beam scanners cause image deformation by mirror induced focal point shifting as shown in FIG. (10).

The first design used the parallel beam scan technique. It quickly became apparent that alignment of the system would be tedious and unproductive. Two considerations prompted a switch to the simpler convergent beam scanner.

First, to allow rapid scan speeds, the two attached mirrors had to be small due to inertia considerations. The type (i) is a circle 2.54 cm in diameter and the type (ii) a rectangle with dimensions 3.3 cm by 3.94 cm. With the Dahl-Kirkham exit beam aperture diameter equal to 3.2 cm, and both mirrors stationary positions being at 45 degrees in relation to the exit beam, the mirror motions must be kept small in order that they present a sufficient cross section to the image beam.

Secondly, the Dahl-Kirkham telescope has a 25.4 cm back focal length for an object at infinity as measured from the primary mirror. If the scanning system could be located close to the exit aperture, it would be (due to the long back focal length) operating in a region where the image beam was nearly parallel.

Because of the necessity for small mirror motions and the long focal length, the use of the convergent beam technique would not cause unacceptable image blur through beam defocus. Consequently, the convergent beam scan system was settled upon as the system for the FLIR.

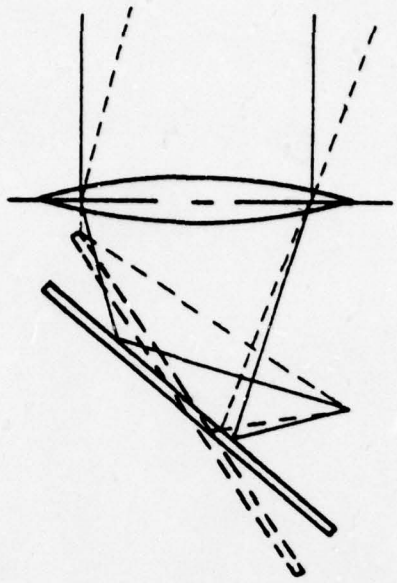

FIG. (9) Convergent Beam Scanning System

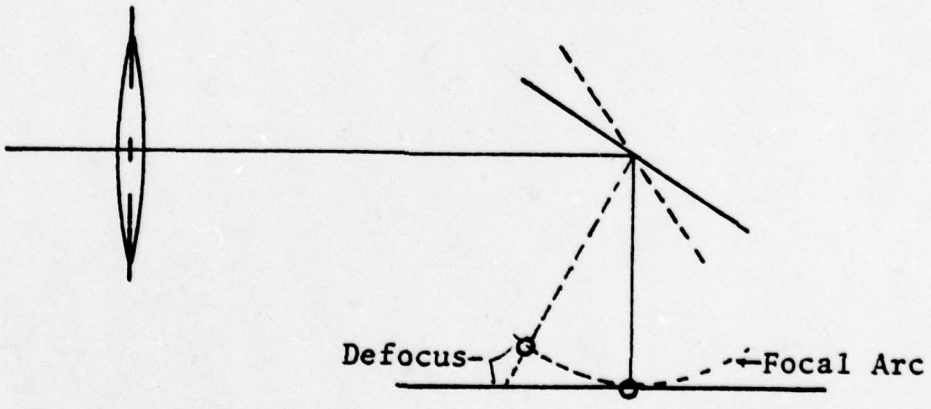

FIG. (10) Convergent Scan Defocusing

2. Raster

The raster consists of two orthogonal linear motions. The high speed scan is fixed near its maximum value for linear sinusoidal frequency response. The fast scan is set at 200 Hz in an asymmetrical sawtooth pattern.

E. W. Engstrum, Ref (2), in a study of television characteristics, concluded that the ratio of lines per picture height has a definite impact on visual acceptability. He found that a ratio of 240 lines per picture is satisfactory, 180 lines is marginal, 120 lines barely acceptable while 60 lines is totally inadequate. Given a fast scan rate of 200 lines per second, to optimize the raster at greater than 240 lines per picture means that the slow scan must have at least a 1.2 second interval excluding flyback time. This value being well within the capability of the slow scan mirror was set to a value of 1.5 seconds with a flyback time of .5 seconds. This is proportional to a .5 Hz frame rate and 300 lines per picture height. As with the fast scan, an asymmetrical sawtooth is used. This was one area where the human/machine interface was amenable to optimization.

While it is undesirable for the operator to perceive the raster, it is visible on the screen as a line which slowly moves down the screen, painting the video picture.

C. DETECTORS

Any consideration of detectors must first start with a decision as to the particular wavelengths to be covered. For military FLIRs, the regions 3-5 μm and 8-12 μm are of particular interest. However, to simplify alignment and speed the design process, the first wavelengths investigated were in the visible.

State-of-the-art FLIRs use linear arrays with full field planar arrays still in the future. Fortunately, the two single cell detectors, manufactured by Santa Barbara Research, Inc., were modern, high detectivity and fast response-time detectors. They consist of a Mercury Cadmium Telluride (HgCdTe) and an Indium Antimonide (InSb) detector having circular dimensions of 2 mm. They are mounted in side-looking dewars and utilize liquid nitrogen cooling to $77^{o}K$. The dewars are capable of a minimum of four hours nitrogen hold time. The HgCdTe detector operates in the 8-14 μm region and is equipped with an IRTRAN 2 window. The InSb (PV) detector operates in the 3-5 μm band and is equipped with a sapphire window. Figures (11) and (12) show some of the IR detectors' operating characteristics.

In the visible range, a silicon avalanche diode is used. It has a range out to approximately 1.1 μm as shown in FIG. (13).

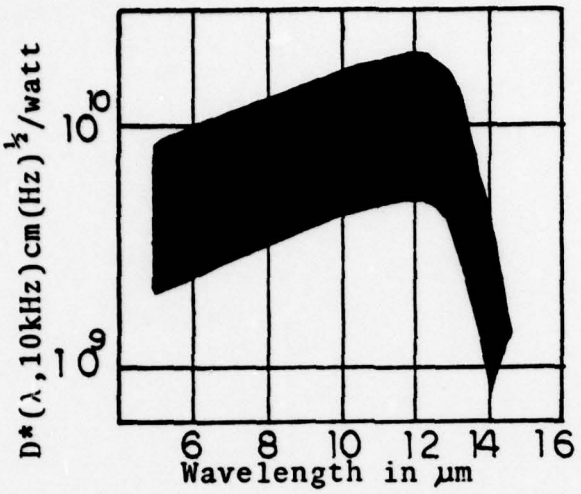

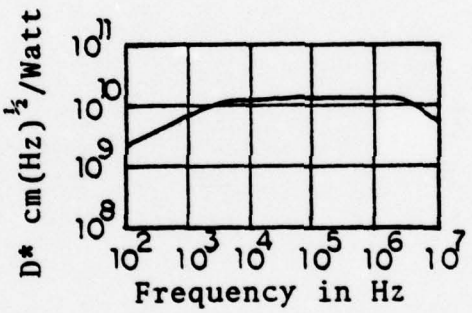

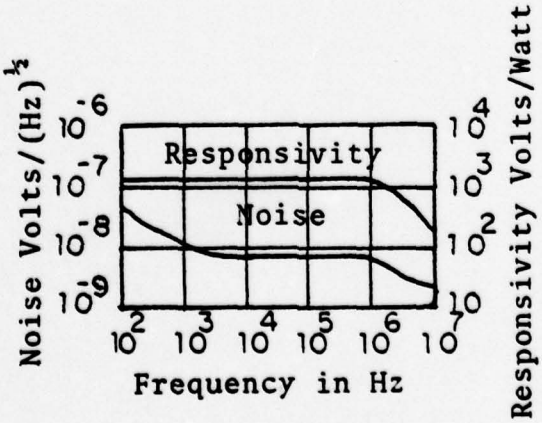

FIG. (11) HgCdTe Detector Characteristics

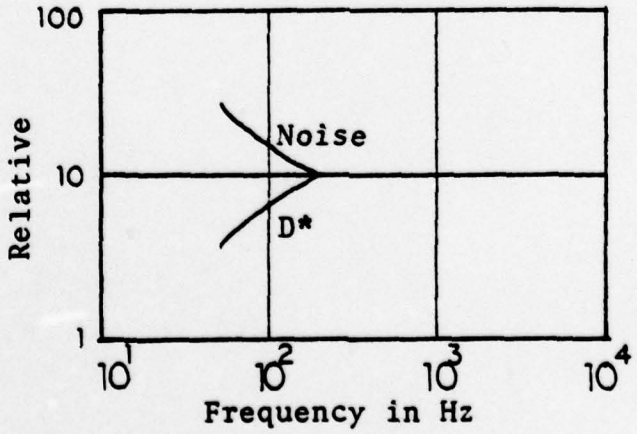

FIG. (12) InSb Detector Characteristics

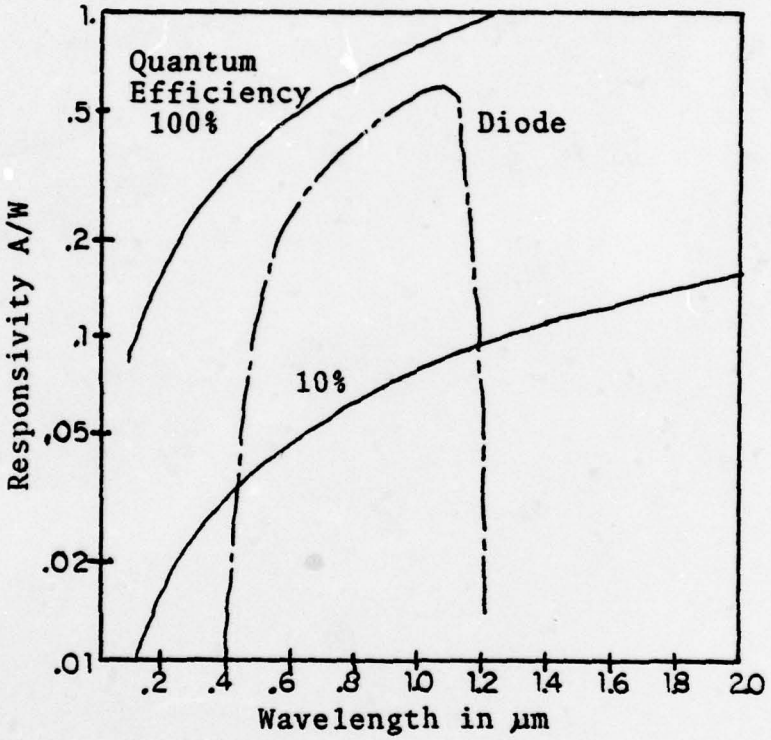

FIG. (13) Silicon Avalanche Diode Characteristic

The angular projection of a detector with dimension,a, through an optical system with an effective focal length,f, is: $d = a/f$

When using a focal plane baffle, the quantity,a, becomes the exposed detector dimension. Reducing the detector size reduces the instantaneous field of view and thus increases the resolution of the system. A smaller detector size also reduces the random detector noise, thus increasing the signal to noise ratio, provided that the background radiation noise is dominant.

Reference 3 describes a commercial, single-cell detector FLIR which uses a circular detector with a diameter of .005 cm. Utilizing this as a target dimension, the three detectors with 2 mm diameter dimensions have surfaces 40 times larger than desired. The larger dimensions, while simplifying alignment, reduce the resolution of the system. Two possible methods for decreasing detector size are (i) smaller active area of detector or (ii) occluding most of the large detector active area with a baffle. The latter method was chosen, and small pinholes, using a #80 drill, were manufactured and positioned over the center of each detector. A #80 drill, the smallest commercially available, has a diameter of .0343 cm and while this is still seven times larger than the targeted .005 cm, it is acceptable.

Another factor which has to be considered with the detectors is the response time in relation to scan speed.

The dwell time of a single cell detector in a scanning system is given by:

$$Td = \frac{\sigma}{AF}$$

where: σ = one dimensional instantaneous field of view
A = one dimensional total field of view
F = 1/Tf
Tf = single line scan time
Td = dwell time

For the system:

σ = .15 milliradians
A = 13 milliradians
F = 200 1/sec
Td = 58 usec

HgCdTe has a response time of 100-800 nsec and InSb has a response time of approximately 1 usec. With the dwell time a minimum of 58 times longer than the slowest response time there are no problems in this area.

D. ELECTRONICS

The major thrust of the electronics suite was to keep it as simple as possible while still providing the necessary services for the optical portions of the system.

The electronics package is broken down into two sections: mirror scan drive and detector/video support. The mirror scan drive section provides drive power signals to the mirrors and scan control signals to the video system.

1. Mirror Scan Drive

A Wavetech function generator provides two asymmetric sawtooths to generate the raster. In addition, it

generates a control pulse which is used for video flyback blanking. TABLE (II) lists all the components of each area.

The raster signals are fed to a synchro control unit and a power amplifier which provide drive power to the mirrors. The fast scan mirror, due to its feedback control system, requires a special scanner control unit while the slow scan mirror utilizes a HP 467A DC power amplifier.

The response of the mirrors to the raster signal has an inherent time delay. In an attempt to avoid this lag interfering with proper synchronization between video signal and video raster, the fast scan signal for the video is taken from the position feedback signal from the fast scan mirror. This signal is available at the synchro scanner control. This type of position signal is not available with the slow scan nonfeedback mirror, so that the slow scan raster signal comes from the HP 467A DC amplifier.

EQUIPMENT	USE
Mirror Support	
Wavetech Model 184 Function Generator	Raster Control
General Scanning CCX101 Scanner Control	Fast Mirror Drive
Hewlett Packard 467A Power Amp.	Slow Mirror Drive
Detector/Video Support	
Interstate Elect. Corp. P12 Pulse Generator	Flyback Blanking

(cont.)

EQUIPMENT	USE
Princeton Applied Research Model 113 Preamp	Detector Signal Amp.
Hewlett Packard 465A Power Amp.	Video Signal Amp.
Hewlett Packard 467A Power Amp.	Blanking Signal Amp.
Monsanto OS-226 (P)/USM-368 Oscilloscope	Display

TABLE (II) FLIR Electronic Equipment

2. Detector/Video

In the video section, the most important component is the display unit. The display unit has to be able to utilize adjustable scan signals in two dimensions and be capable of beam intensity modulation. In addition, the screen has to have a fairly long decay phosphor to compensate for the slow frame time. The oscilloscope listed in TABLE (II) meets all these requirements nicely.

To obtain useable signals from the detectors, each requires different biasing and/or power supply arrangements. The InSb (PV) detector is operated into a 300 MegOhm input resistance around a bias voltage of 0; FIG (14). The HgCdTe detector is photoconductive, which means a conduction current is necessary, while the avalanche photodiode operates near breakdown and requires 156 volts. Figure (15), (16), and (17) detail the requisite circuits.

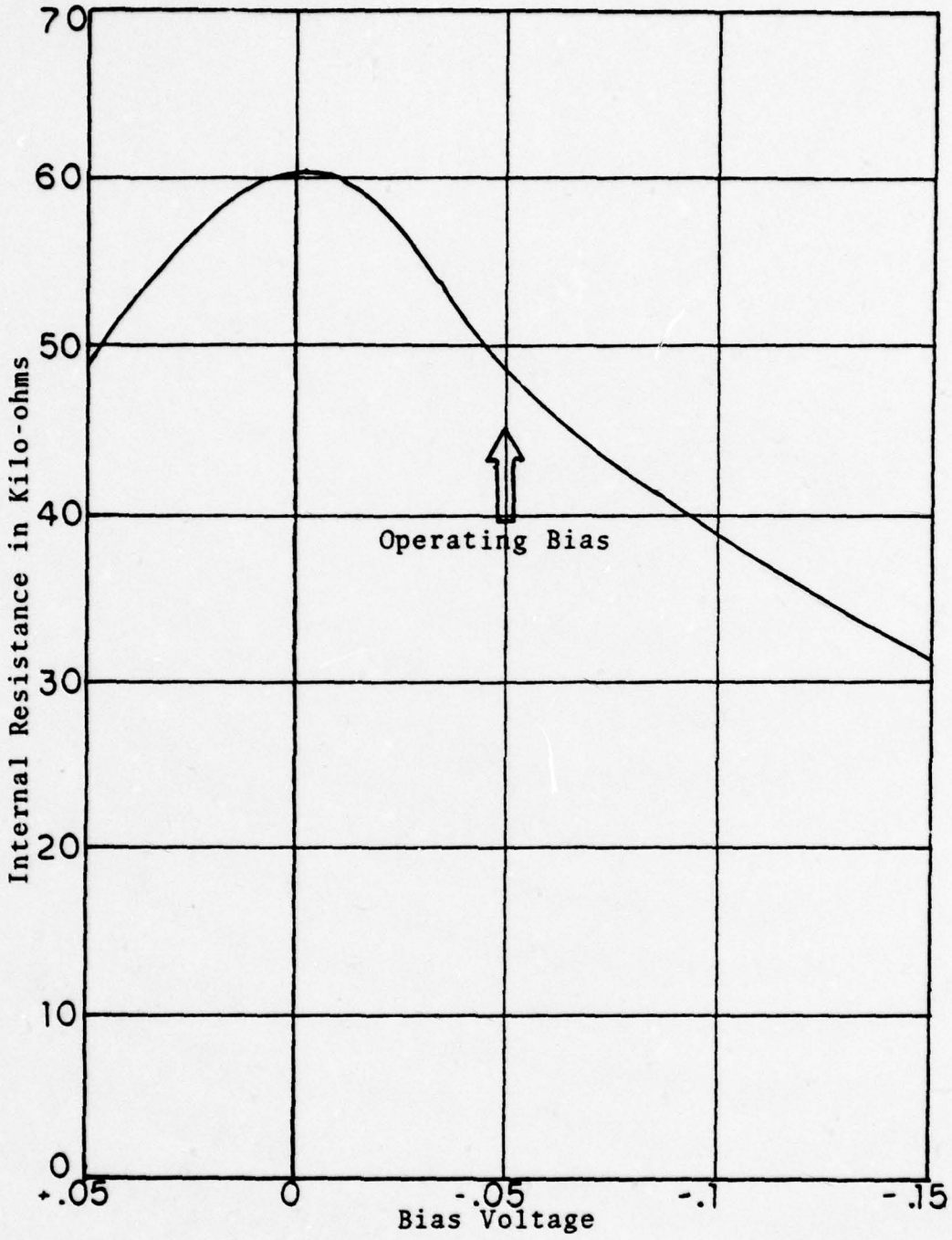

FIG. (14) Internal Resistance as a Function of Bias Voltage for the InSb Photovoltaic Cell

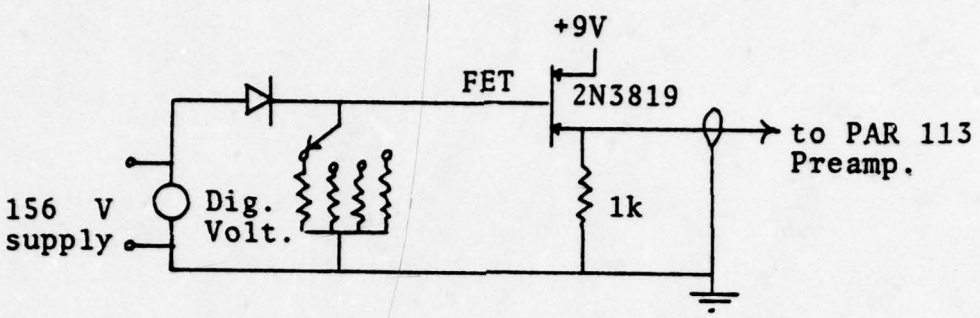

FIG. (15) Circuit for Avalanche Detectors

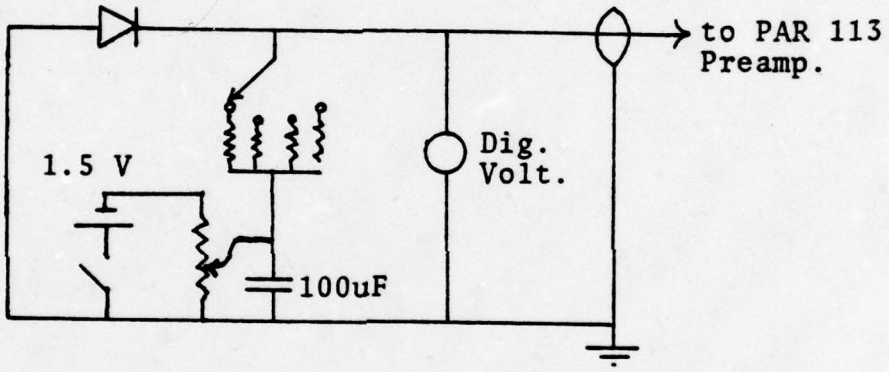

FIG. (16) Circuit for InSb Photovoltaic Cell

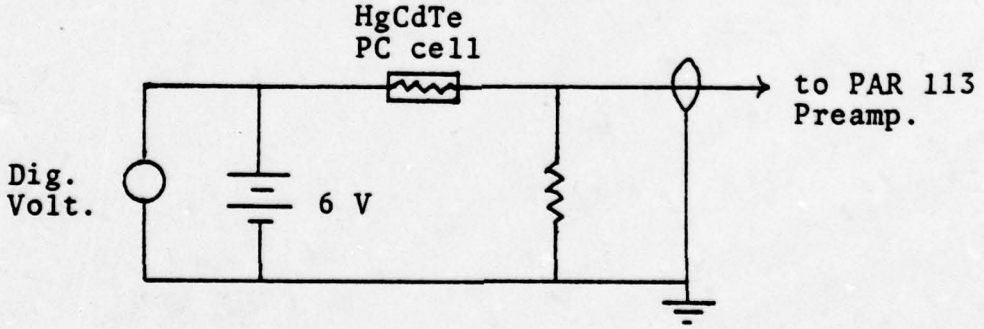

FIG. (17) Circuit for HgCdTe Photoconductive Cell

All three detector outputs are fed into a PAR 113 high gain preamp which normally would provide all the necessary amplification. However, the fact that the signal is required to modulate the beam intensity for the oscillo - scope means that an additional stage of amplification is necessary. The second stage of amplification is accomplished by a HP 465A DC power amplifier which can provide 40 db of gain to comparatively high voltage levels without saturation.

To provide for a more acceptable video display, the screen is blanked during the slow scan flyback time. Only the slow scan flyback is blanked; the fast scan flyback does not cause any noticeable interference.

Blanking is accomplished by a pulse generator triggered from the function generator, which then outputs a single pulse of the proper dimensions. Since the oscilloscope operates on the principle that a negative voltage is proportional to the brightness level, the pulse generator has to produce a positive pulse. For the Monsanto Oscilloscope a minimum voltage of +10 volts is required to cause blanking.

Due to impedence mismatching at the oscilloscope Z input, a diode was inserted between the HP 467A and the Z input junction. The diode allows the pulse to pass while preventing signal loss to the pulse generator from the HP 465A signal amplifier. The HP 467A pulse generator

amplifier was added to increase the blanking pulse's amplitude. This is required because the pulse generator is capable of a maximum pulse amplitude of 10 volts and it is attenuated by the diode below useable levels.

IV. RESULTS

A. VISIBLE

After ensuring that the individual subsystems operated properly, they were integrated into the FLIR system. As discussed previously, the first imaging attempts took place using the silicon avalanche photodiode in the visible region.

Figure (18) shows the target for the first imaging attempts. It was located at the end of a passageway, 132 m from the system. Initial scene illumination was one 100 watt incandescent light bulb.

Utilizing a ground-glass screen, and slowing down the fast scan mirror, allowed the field of view to be measured. At 132 meters the field scanned was 83.8 cm by 38.1 cm which is proportional to a 6 milliradian by 3 milliradian field of view. Normal mirror scan frequencies during this time were 160 Hz and 3 Hz.

Figure (19) shows the first recognizable video image produced by the system. It is the 100 watt light bulb and its white reflector, which had been turned to shine directly toward the telescope, seen through the vertical slats of a wooden chair. In this case, the detector was fitted with a .034 cm pinhole.

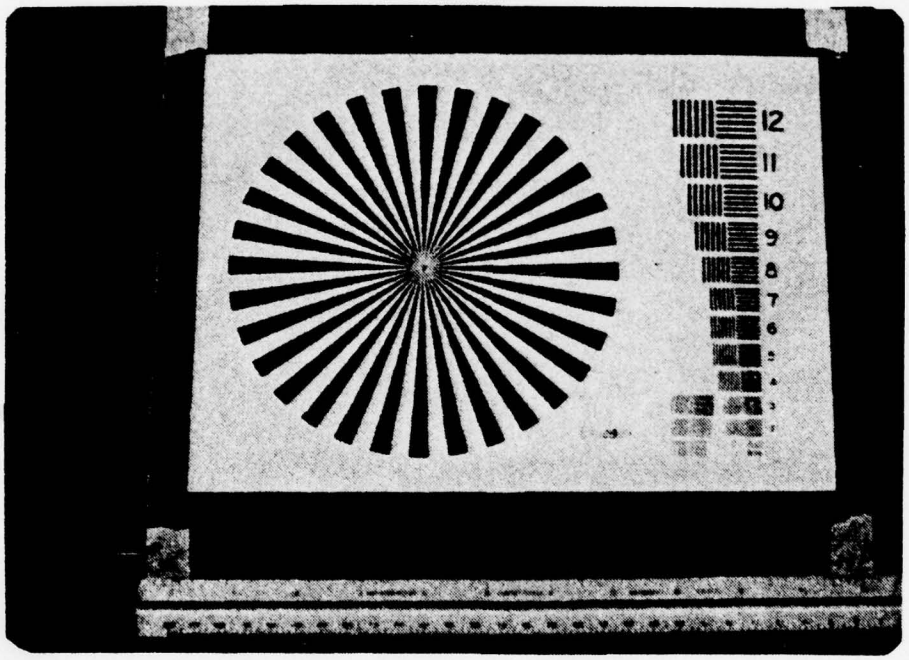

FIG. (18) Visible Light Target

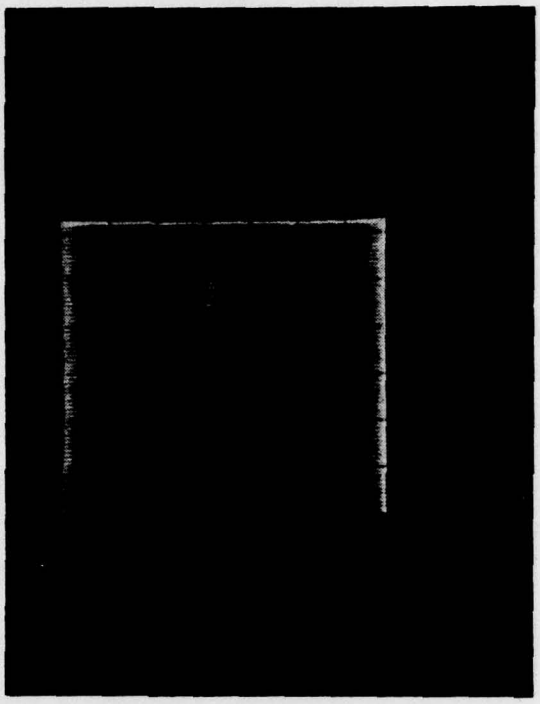

FIG. (19) First Visible Light Image. Incandescent light bulb seen through vertical chair slats.

FIG. (20) Visible light target and reflector backs. 64 Meters.

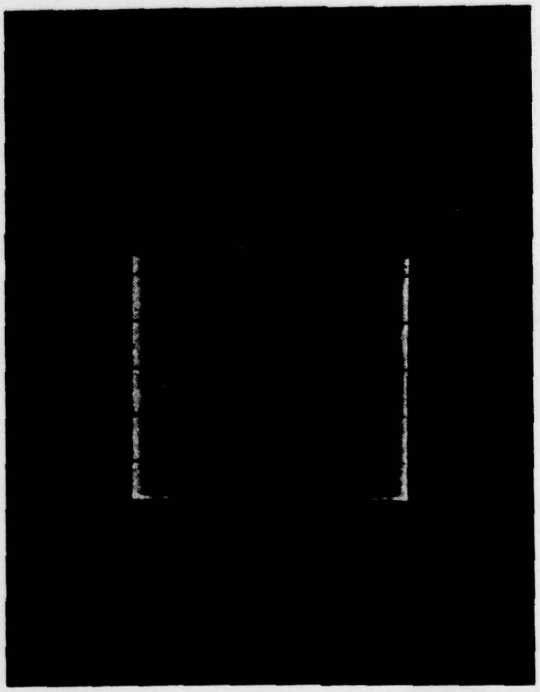

Since scene illumination and received light power are limiting factors, two additional 100 watt light bulbs were added for illumination and the target was repositioned to a distance of 64 m from the system. Figure (20) shows the results. Clearly visible are the three light reflector backs as well as the resolution chart.

Picture size and intensity can be controlled by adjustments to oscilloscope controls and amplifier gain. Subsequent pictures were expanded to fill the entire oscilloscope screen. Examination of the initial pictures indicated that the field of view had expanded to 13 milliradians by 10 milliradians. This was due to the change in scan system type and its movement closer to the optics exit aperture.

During the next few days, the emphasis shifted to optimizing the picture appearance through the use of available controls and pinhole sizes. Figures (21) and (22) show the difference in resolution caused by changing the pinhole diameters. The .034 cm pinhole produced clearer images and was accepted as the standard for subsequent experiments.

Figures (23) and (24) illustrate the effect varying the slow scan speeds has on the video. In the top picture, the slow scan has been speeded up such that the fast scan raster is visible. In the bottom picture, the slow scan speed is such that the number of horizontal lines

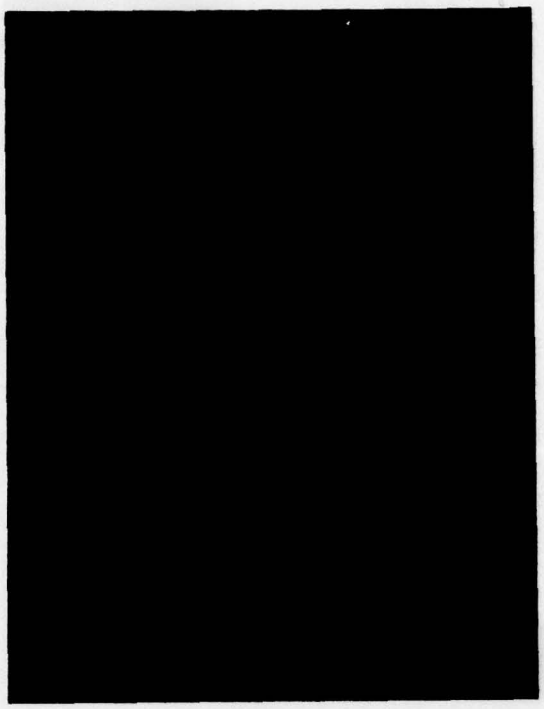

FIG. (21) Target using .034 cm pinhole.

FIG. (22) Target using .053 cm pinhole.

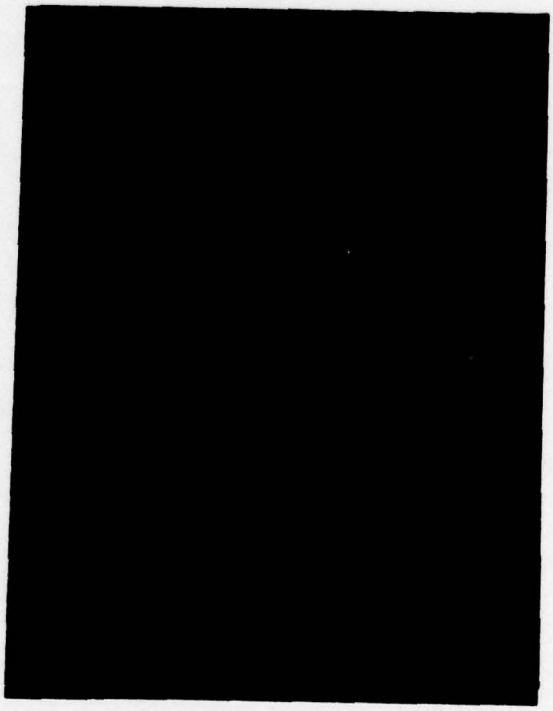

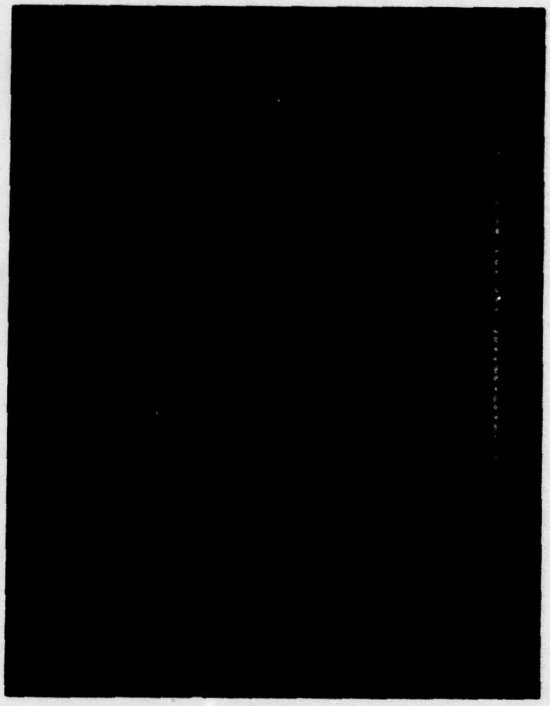

FIG. (23) Target seen with slow scan speed of 3 Hz. The fast scan raster is visible.

FIG. (24) Target with slow scan speed of .5 Hz. No raster noticeable.

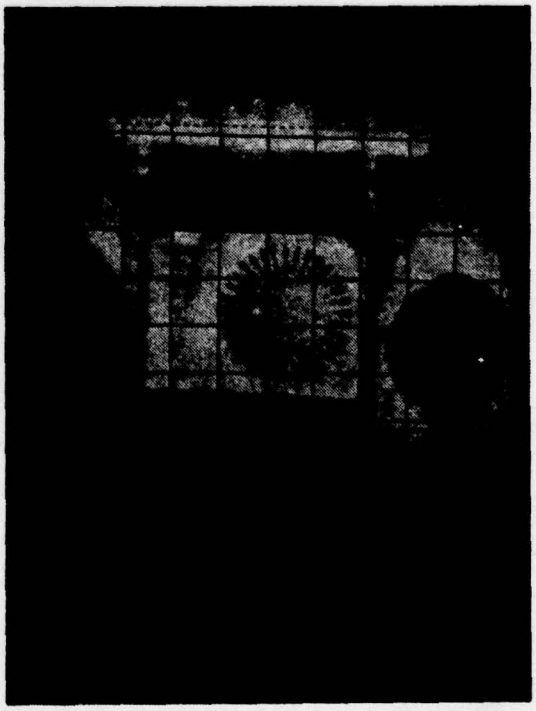

is greater than 240. As previously discussed, this figure of 240 lines per picture provides an acceptable image. These pictures verify the results reported by E. W. Engstrom in Reference 3.

All the pictures from the system used exposure times averaging 60 seconds which had the effect of integrating many pictures. This integration eliminated any slow scan raster perception. To the observer, however, the slow scan was clearly visible as a line which moved down the screen, painting the video image. The perception of the scan was not annoying and after several minutes viewing was not consciously visible. The picture on the screen was clearly visible and recognizable after a single pass of the slow scan, due in part to the long persistance of the screen phosphor and the ability of the eye to integrate a signal extended in time and space.

B. INFRARED

With success in the visible wavelengths and a better understanding of the interrelation of the individual subsystems to overall system performance, work was started to switch over to the infrared bands. Due to dewar design, it was at first deemed impractical to locate a pinhole close enough to the detector.

The first infrared imaging attempt was made by using one of the 2.54 cm focal length germanium lenses

to focus the image of the pinhole, which was physically located at the focal plane of the front end optics, onto the detector. The detector used was the HgCdTe (8-12 μm) detector.

The targets for the initial attempts were as shown in FIG (25). The soldering iron and heating element were the IR targets while the incandescent bulb was used to check scan system alignment.

After several unsuccessful tries, the images of FIG. (26) were produced. The U-shaped heating element is clearly visible, as is the soldering iron more faintly to the left side of the picture. The bright spot in the center is apparently the hot filament of the light bulb as seen through the glass. The double images and blurring were caused by slight misalignment of the lens and the fast scan flyback.

Using a Chromel P-Alumel thermocouple the temperatures of the targets were ascertained and are listed in TABLE (III) below; background temperatures were on the order of 295°K.

HEATING ELEMENT	755°K	$\Delta T = 460^{\circ}K$
SOLDERING IRON	673°K	$\Delta T = 378^{\circ}K$

TABLE (III): Target Temperatures

Appendix A contains energy calculations for the received energy from these temperature targets.

At about the same time as the images were being produced, it proved feasible to equip the IR detectors with pinholes close to the detector surfaces. This eliminated the need for the germanium lens and the alignment procedures.

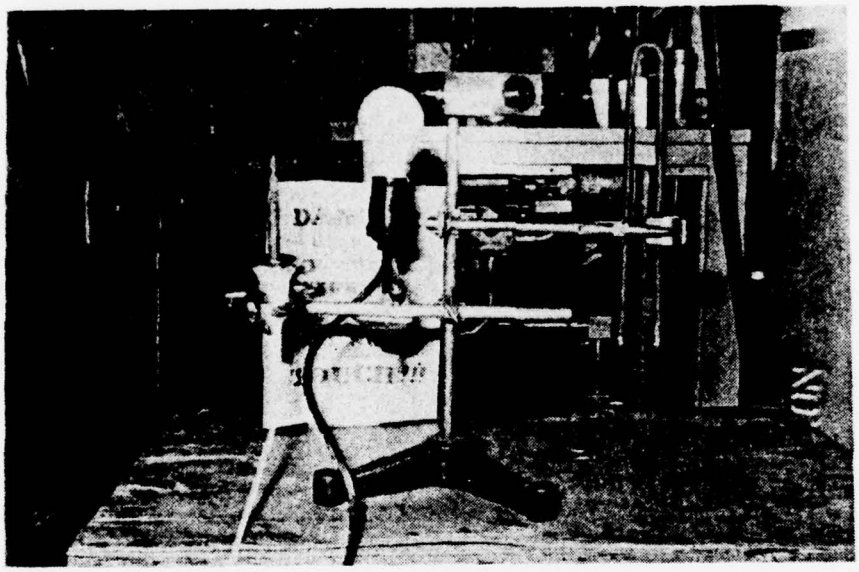

FIG. (25) Infrared Targets

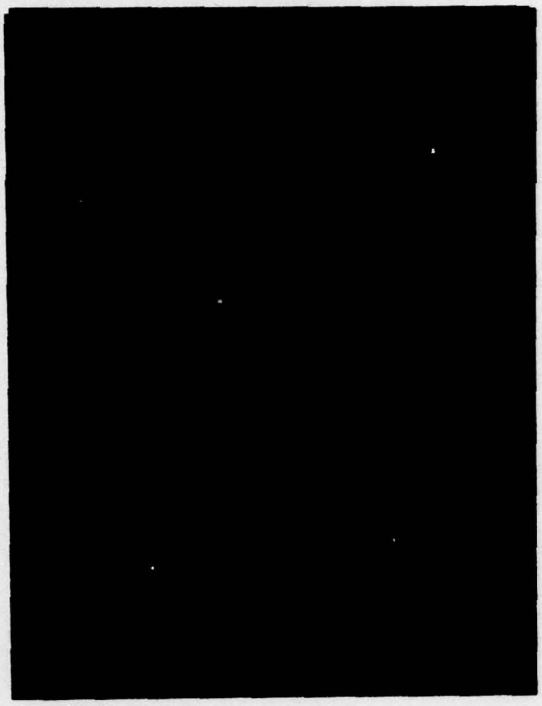

FIG. (26) First Infrared Images in the 8-12 um band.

FIG. (27) Images with the new pinholes installed.

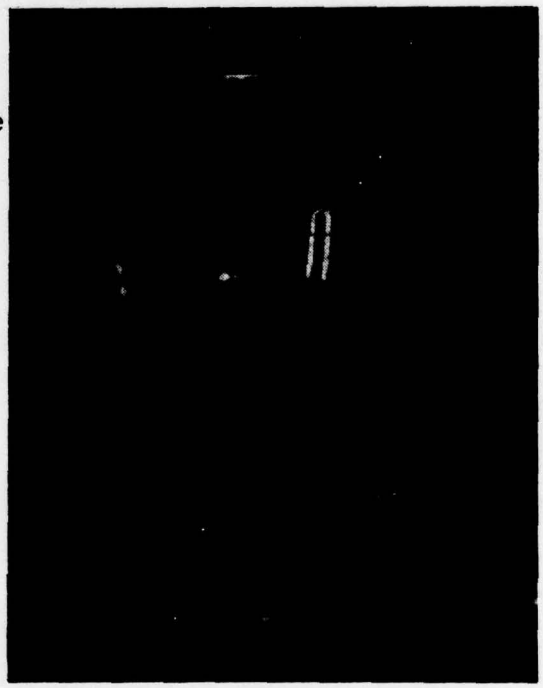

The pinhole size was the previously utilized .034 cm diameter pinhole. Figure (27) shows the results from this arrangement. In this second picture, the images are much sharper and clearer. Even the reflector, which was present for this group of pictures, is faintly visible behind the filament hot spot.

In figures (28-30) various target aspects and ranges were studied for their effect on scene recognition. As in the previous pictures, the slow scan is from top to bottom with the fast scan from left to right. Sixty seconds average exposure time for the photographs caused scene integration. All pictures were visible and recognizable after a single frame. The scan speeds were 200 Hz and .5 Hz.

The heating element's temperature was adjusted downward and every effort was made at the system to maintain the image; including increasing the PAR 113's gain. During this experiment the temperature at which the image of the heating element disappeared into the background noise was $365^{o}K$, $\Delta T = 70^{o}K$.

The light and dark bands across the picture face were at first thought to be attributable to NON DC Restoration (Ref. 1). However, they were later traced to an electrical problem.

The electrical problem first surfaced when the InSb detector was used. Figure (31) shows the target images as recognizable but blurred and with the heating element cut

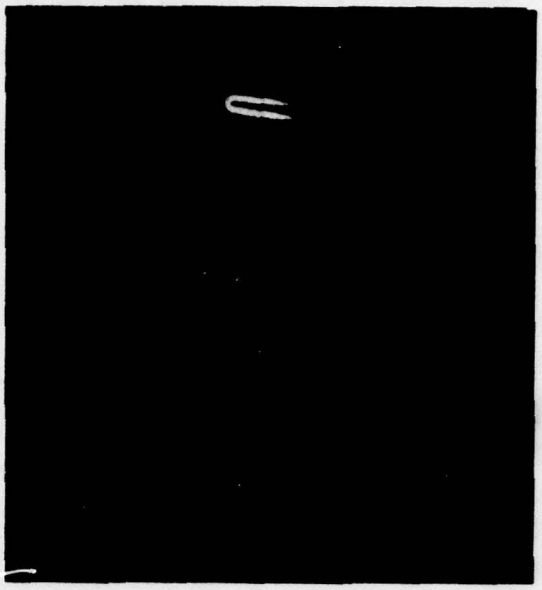

FIG. (28) Targets at
64 M. HgCdTe detector.

FIG. (29) Target at
32.6 M. HgCdTe detector.

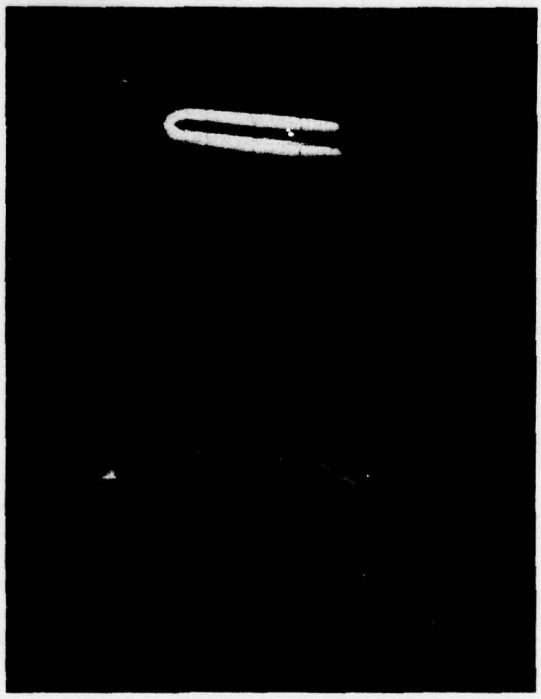

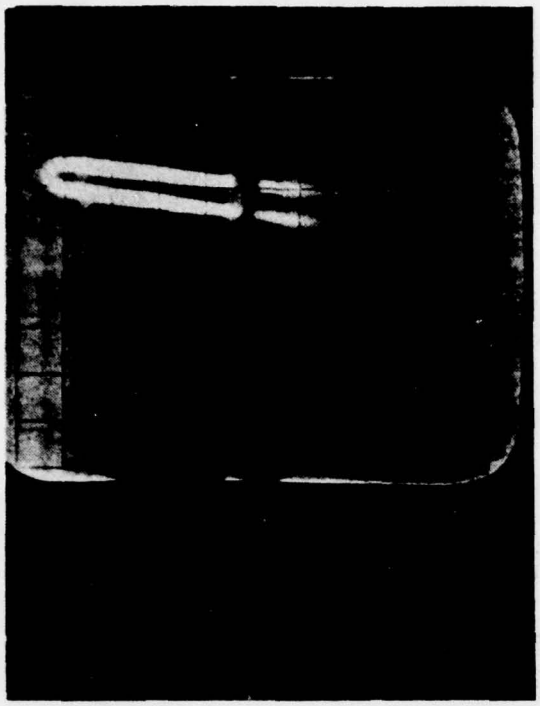

FIG. (30) Target at 32.6 M. HgCdTe detector.

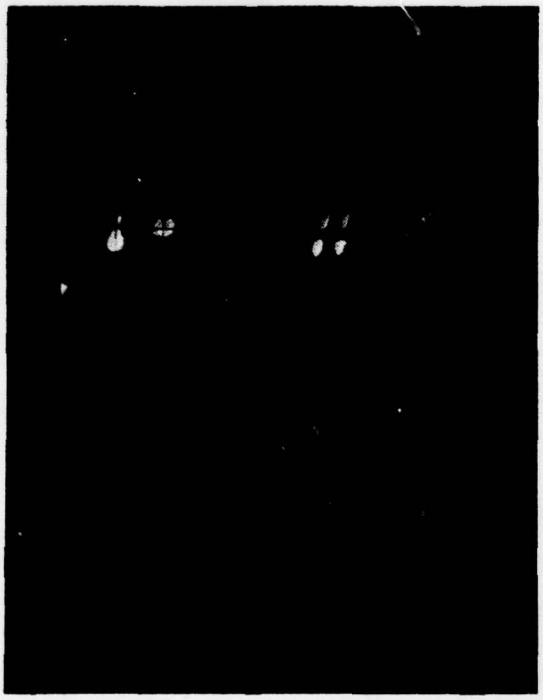

FIG. (31) InSb detector first attempt showing impedence mismatch problem.

off at its top. Figure (32) shows the same scene with the blanking pulse generator disconnected and the PAR 113's gain reduced. The shadow behind and to the upper right of the heating element was caused by the unblanked slow scan flyback. The problem turned out to be an impedence mismatch the correction of which, as previously discussed in section III D, involved the insertion of a diode. As can be seen in FIG. (33), this small correction resulted in a significant improvement in image quality.

With the complete system in operation, measurements were once again conducted to determine the minimum discernable temperature difference of the system in each frequency range. The target was the heating element controlled by a powerstat. An attached Chromel P-Alumel thermocouple was used for the temperature indicator.

Using the HgCdTe detector, the element was discernable down to a temperature of $304^{o}K$, $\Delta T = 9^{o}K$, at 65.5 meters. The InSb detector did not do as well and the image was lost when the temperature reached $391^{o}K$, $\Delta T = 96^{o}K$. Appendix A gives the energy calculations for these two temperatures.

It is interesting to note that while the InSb has the highest D*, it did not achieve the lowest temperature reading. The reason for this apparently lies in the power in the region in which each detector operates. As can be seen by the calculations in Appendix A, the InSb detector received less power by a factor of two. While a

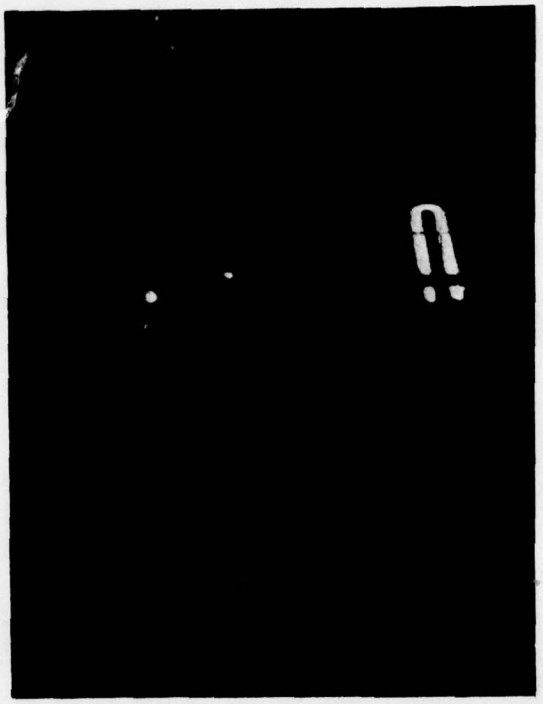

FIG. (32) InSb detector
Pulse Generator disconnected.

FIG. (33) HgCdTe detector
with corrected impedence.

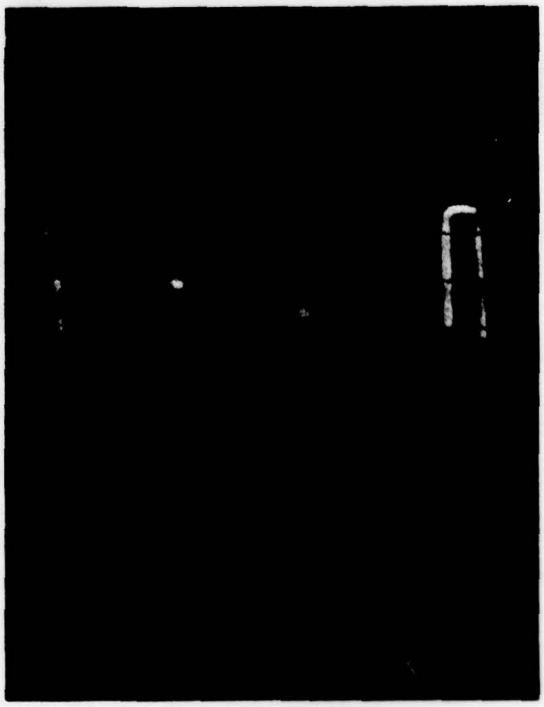

comparison of the detectors' D*s would show that the InSb detector has a factor of 10 improvement over the HgCdTe detector and thus should have done better, it is not true in this case. The HgCdTe detector used in these experiments was more sensitive than the standards shown in FIG. (11) by nearly that same factor of 10, thus explaining the apparent discrepency.

In both of the minimum temperature experiments, the PAR 113's gain was increased as signal power was reduced until the image was lost in the background noise level.

C. MTF CALCULATIONS

One final step prior to use of the system upon real world targets was the characterization of system performance through the calculation of its MTF and comparison to the theoretical performance.

The target for this test was a length of #30 Nichrome resistance wire shaped into a rough square, FIG (34), located at 65.5 m from the system. Taking a single scan through the two wires provided the systems impulse response. The wires were small enough in angular dimension to be considered point sources and the two wires, together with their known angular separation, provided a method for self calibration of the oscilloscope pictures.

A graph from the expanded picture of the single wire response, FIG (35), was digitized and used in a Fast

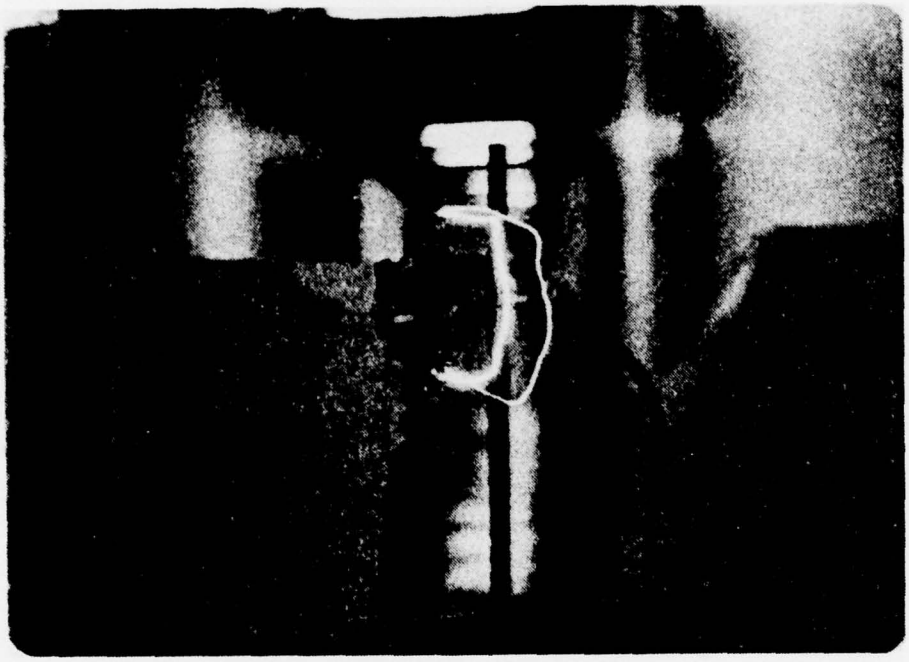

FIG. (34) Nichrome Wire MTF Target

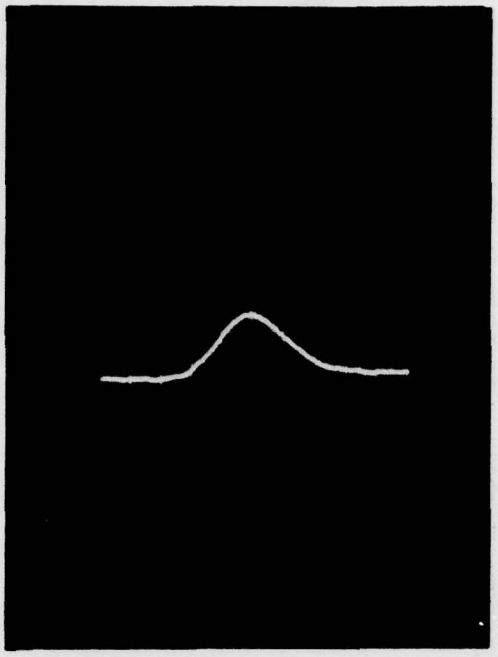

FIG. (35) Single Wire Delta Response

FIG. (36) Enlarged Single Wire Response

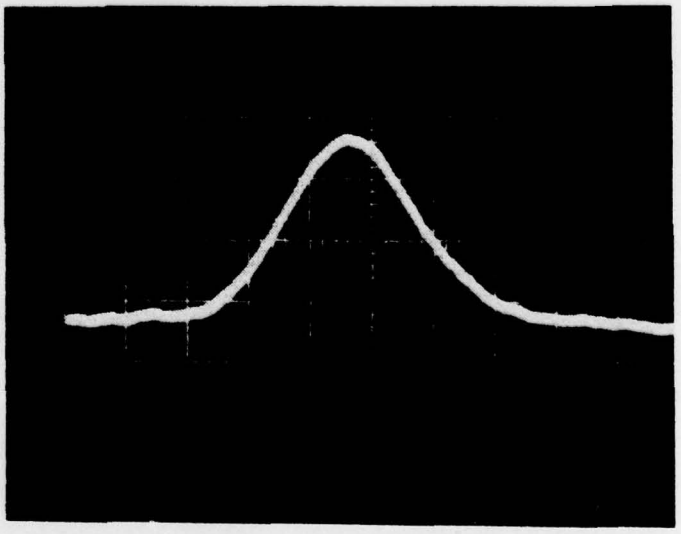

Fourier Transform computer program to obtain the system's MTF.

Utilizing the same Fast Fourier Transform program, the theoretical MTF due to the pinhole Line Spread Function was calculated and plotted as FIG (37).

A different computer program designed by Professor Milne, NPS Department of Physics and Chemistry, was used to calculate the theoretical MTF due to the diffraction Line Spread Function caused by the telescope optics and it is given as FIG (38).

Taking the product of the two theoretical MTFs, which were considered to be the major contributors to overall system MFT, gives the theoretical system MTF.

A comparison of the theoretical and experimental results, FIG (39), shows a good agreement between the two curves. As expected, the experimental results over most of the frequency range indicate that the system does not resolve as well as it theoretically could. It is interesting to note that between 0 and 1.7 milliradians^{-1} the system does slightly better than predicted. It would be interesting to speculate upon the reasons for this phenomenon, but that is beyond the scope of this project.

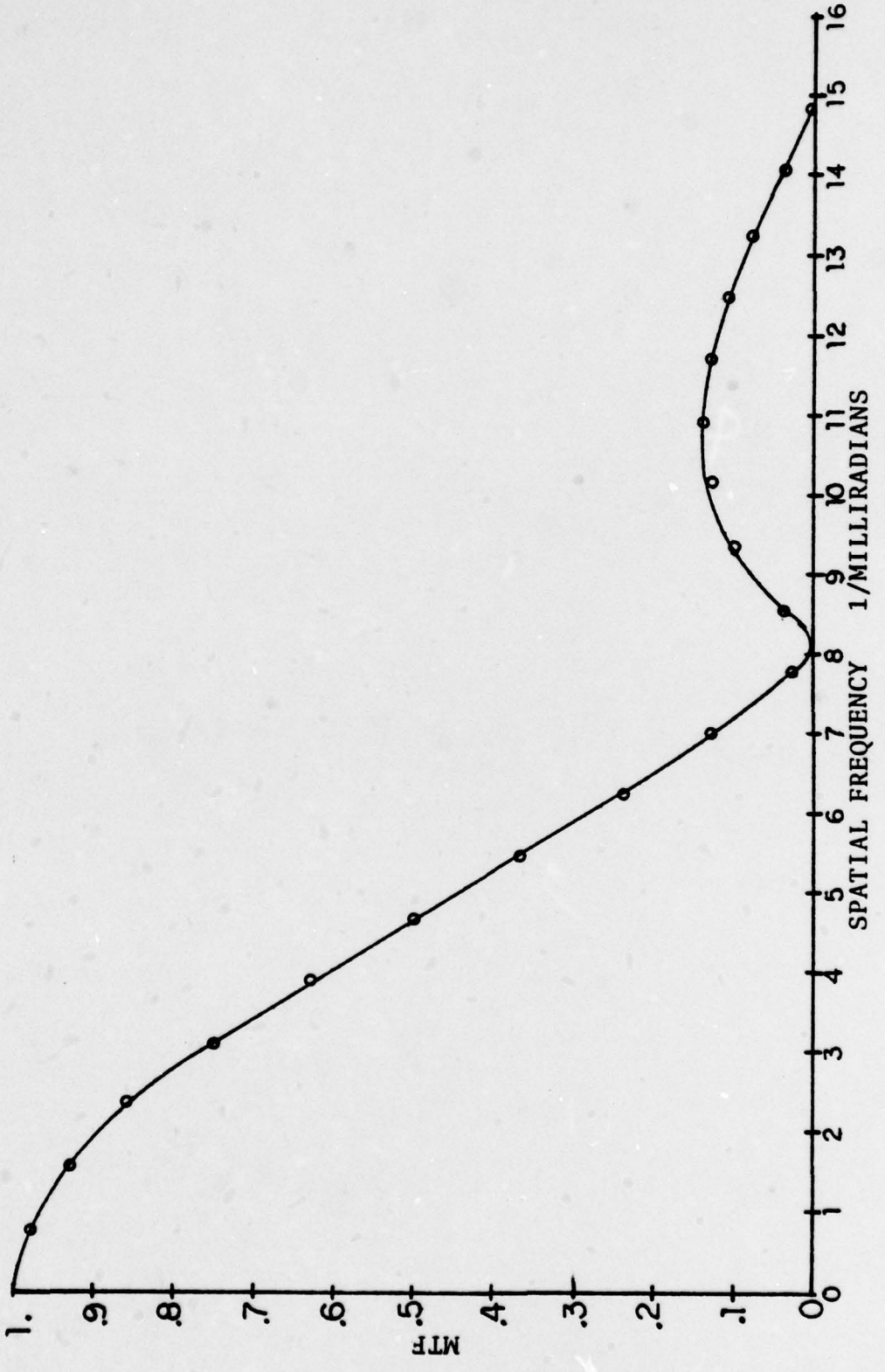

FIG. (37) Theoretical MTF due to Pinhole

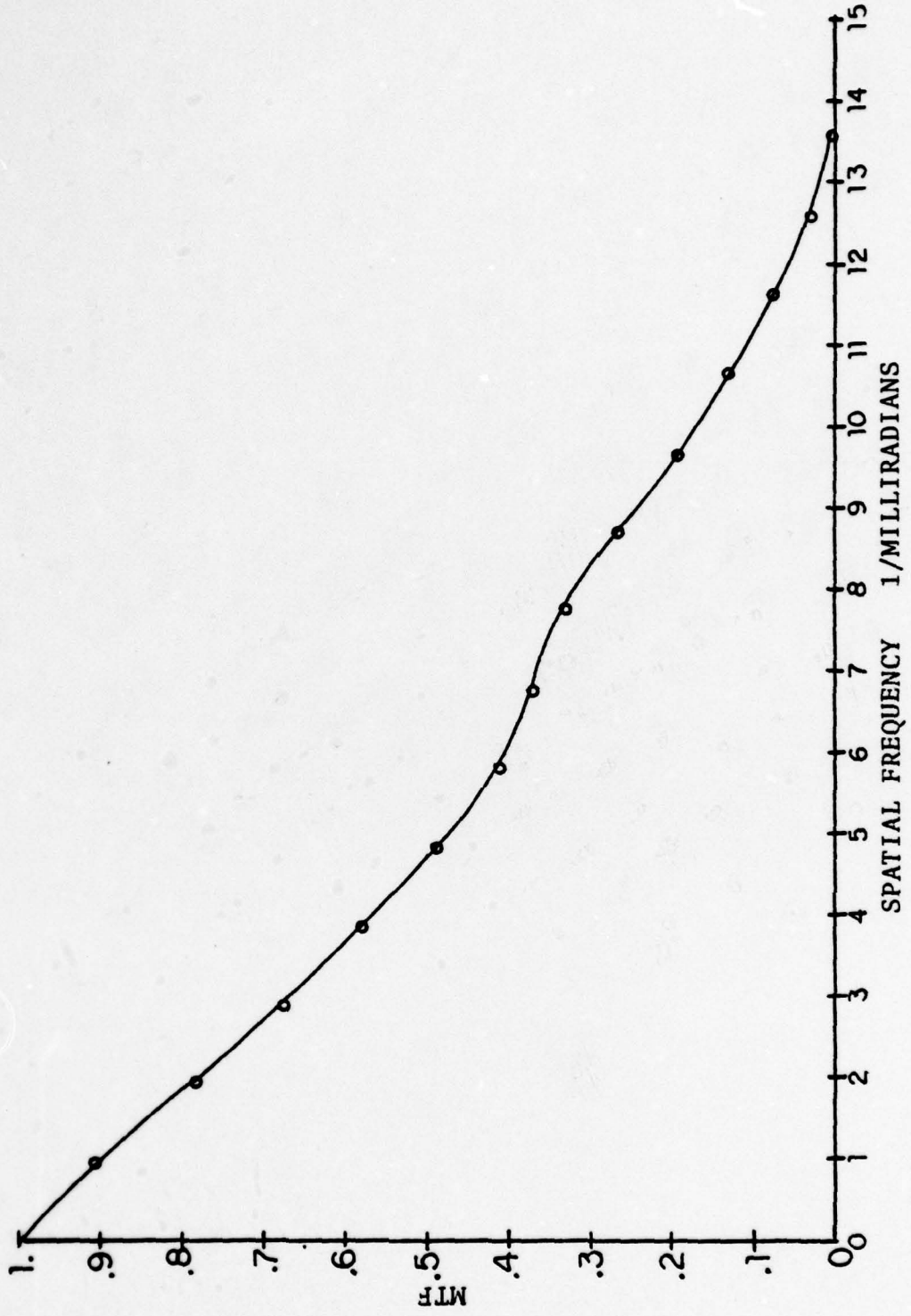

FIG. (38) Theoretical MTF due to Optics Diffraction

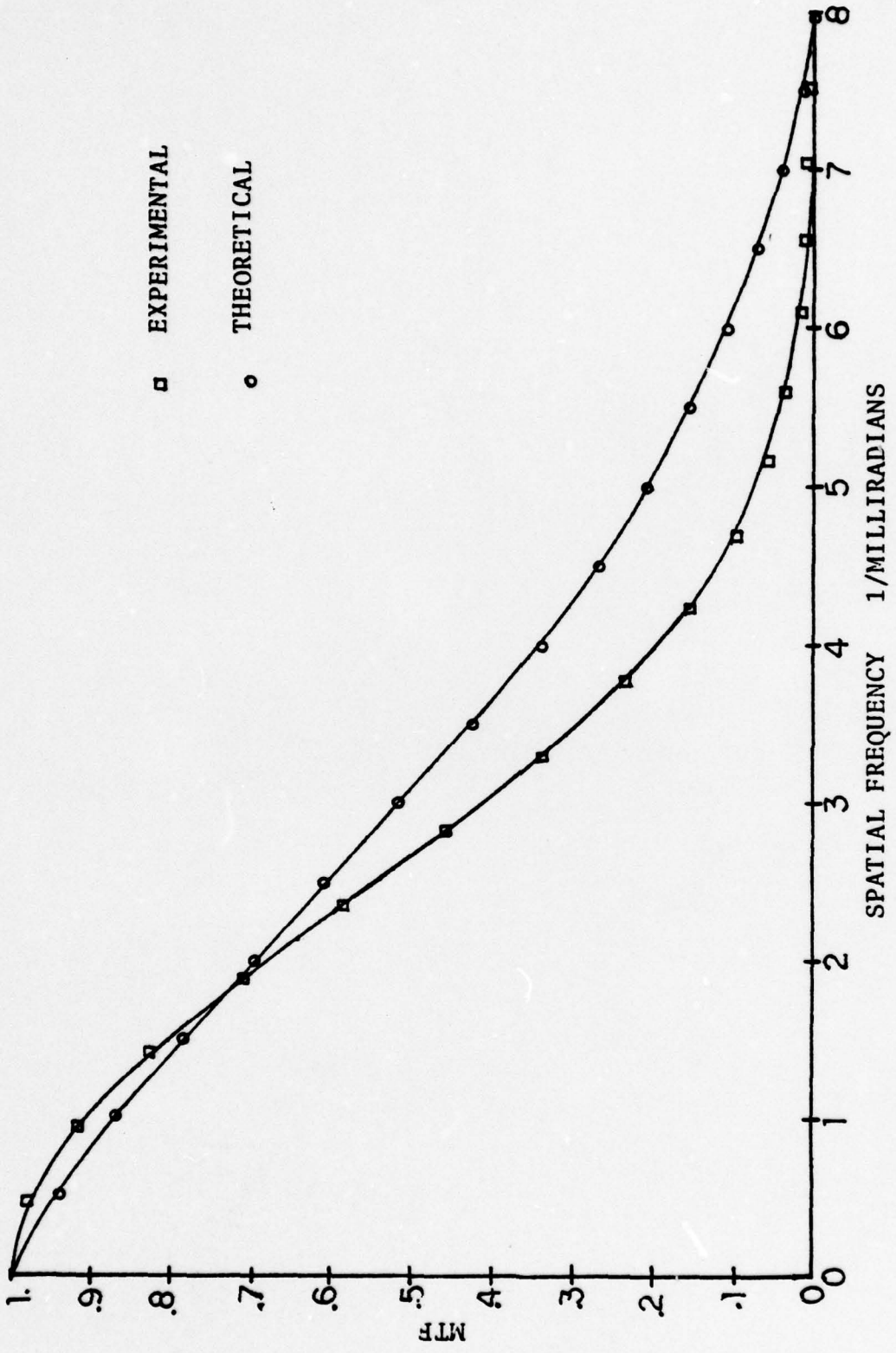

FIG. (39) Comparison of Experimental and Theoretical MTFs

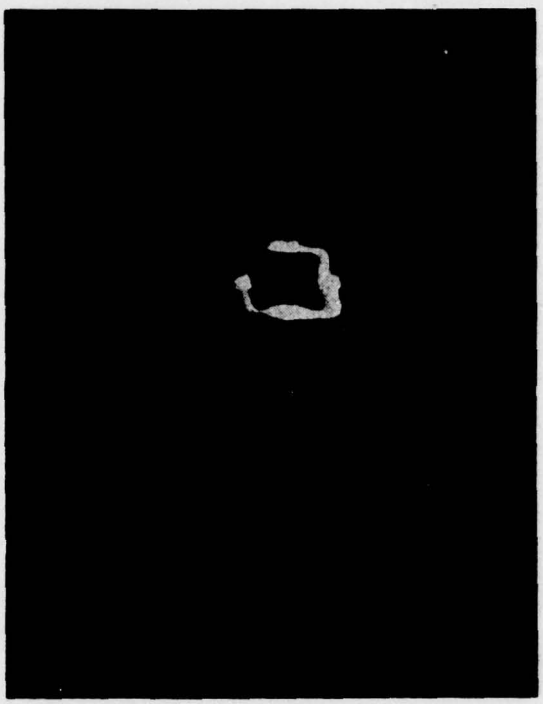

FIG. (40) MTF Target. Bright spots indicate location of single line scan.

FIG. (41) System Target Response.

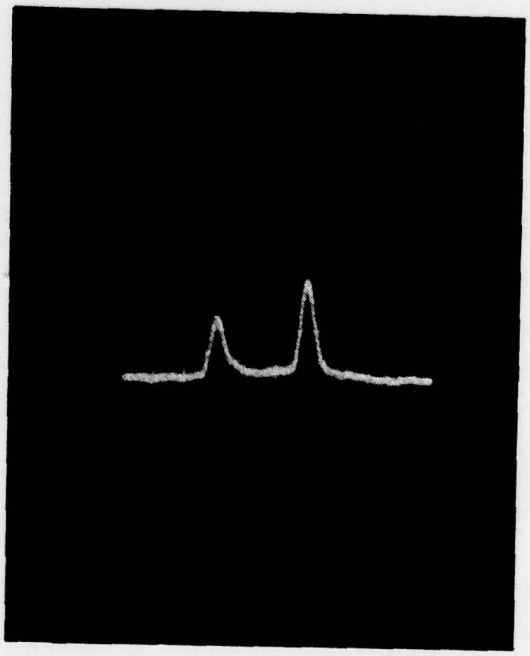

V. SUMMARY

An operating FLIR was designed and constructed utilizing components available at NPS. The device, employing a convergent-beam, mirror scanning system, is totally catoptric and capable of operating over a wide range of electromagnetic wavelengths. It is less sensitive than a completely optimized configuration, but performs about as was expected under the conditions of the trade-offs dictated by the existing components. However, as the first such device physically available at NPS, it has proven invaluable in providing a working knowledge of FLIR problems and principles. The system should prove an excellent platform for further advanced study in the field of thermal imaging.

Lessons learned during the course of this project include the interrelation of systems components as related to resolution, the significant effect that the electronics package has in video signal recognition and, in general, how video systems perform.

VI. AREAS FOR FURTHER STUDY

Though FLIRs are not new, their experimental study at NPS is a new field, and, as with any new endeavour, opportunities abound for further study, research and improvement.

A. IMPROVEMENTS TO THE SINGLE CELL FLIR

There are many areas where the single cell FLIR could be improved. A different optics system, with shorter focal length, would increase the field of view. The scan mirrors should be enlarged to intercept more of the image beam and to allow for larger mirror displacements to increase the field of view; this would necessitate that larger mirror drive motors be provided. The mirror scan system could be redesigned to utilize such devices as rotating drum mirrors, rotating prisms or wedges.

With a redesigned scan system the raster rate could be increased to make it compatable with the standard U.S. TV format. This would enable a TV monitor unit to be used for display.

New detectors of smaller size would increase the signal-to-noise ratio and increase resolution. Other detectors in different wavelengths bands would increase the dynamic range of the FLIR.

B. NEXT GENERATION IMPROVEMENTS

To progress beyond the single cell FLIR would require use of more state-of-the-art equipment and techniques. Linear array detectors and their associated electronics and scan systems are presently commercially available. Full field planar arrays operating on either the CCD or CID principle should be available in the near future. Either type of array would cause a quantum jump in FLIR performance.

Computer enhancement of the video signal is another area where good effort would pay off handsomely in improved performance.

Moving away from scanning systems altogether, the pyroelectric vidicon is pushing to the forefront of the attempts to produce a thermal imager on the same lines as a television camera. Its use is sure to increase with time and should provide an interesting area for study.

C. GENERAL RESEARCH AREAS

In a more general vein, once the operating principles of thermal imagers are more thoroughly understood, it would be extremely beneficial to the NAVY to pursue a study in the trade-offs required to use the different IR wavelengths and styles of FLIR equipments. Another possibility would be a projection on the costs and weights

of planned and projected improvements, as related to mission requirements, to military FLIR systems.

This project has only touched the surface of a rich and varied field of endeavour which is of immense interest to anyone concerned with National Defense. The aforementioned areas are not meant to be comprehensive or all inclusive and should serve merely to stimulate the intellect.

APPENDIX A ENERGY CALCULATIONS

Target -- Inconel Rod

Emissivity = .7 .635 cm diameter

Optics

Instantaneous Field-of View = .15 milliradians square

at 65.5 meters = .965 cm square

The target appears as a flat surface with dimensions;

.635 cm by .965 cm

TEMPERATURE = $755.8^{o}K$

Power in the 8-13 μm band

From universal black body curves 20.5%

of the total power is in the band.

$Mt = \sigma T^4 = 1.84X10^4\ W/m^2\ X\ .7 = 1.28X10^4\ W/m^2$

$M = .205\ X\ Mt = 2.62X10^3\ W/m^2$

Power in the 3-5 μm band

From universal black body curves 32.5%

of the total power is in the band.

$M = 4.21X10^3\ W/m^2$

Assume a Lambertian Surface for the Rod target.

$L = M/PI$

$L(8\text{-}13) = .834X10^3 W/m^2STR$ $L(3\text{-}5) = 1.34X10^3\ W/m^2STR$

Rod = $6.13X10^{-5}$ M^2

I = L X A

I (8-13) = .05 W/STR I (3-5) = .082 W/STR

Solid Angle Subtended

OPTICS 15.24 cm diameter Area = 182.4 cm^2

OBSCURATION 3.49 cm Diameter Area = 9.58 cm^2

at $6.55X10^3$ cm

$\Omega = A/R^2 = 4.2X10^{-6} - .22X10^{-6}$ STR

$= 3.98X10^{-6}$ STR

Received Power at the Aperture

(For a temperature of 755.8°K)

$\Phi = I\Omega$

Φ (8-13) = $1.99X10^{-7}$ WATTS

Φ (3-5) = $3.26X10^{-7}$ WATTS

TEMPERATURE = 304.5°K (HgCdTe Detector minimum detectable)

Power in the 8-13 μm band

From the universal black body curves 34%

of the total power is in the band

Mt = 487 W/m^2

M = 115.9 W/m^2

L = 36.9 W/STR m^2

I = $2.26X10^{-3}$ W/STR

Φ = $8.99X10^{-9}$ WATTS Power received at the aperture

TEMPERATURE = 391^{o}K (InSb Detector minimum detectable)

Power in the 3-5 μm band

From the universal black body curves 6%

of the total power is in the band.

Mt = 1325 W/m^2

M = 55.6 W/m^2

L 17.7 W/m^{2}STR

I = 1.08X10^{-3} W/STR

Φ = 4.32X10^{-9} WATTS Power received at the aperture.

APPENDIX B SYSTEM PHOTOGRAPHS

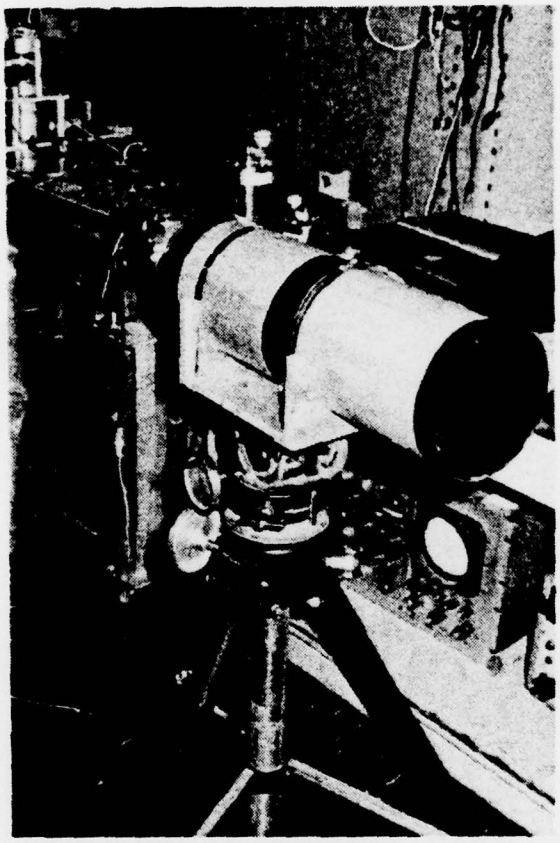

FIG. (42) Optics and Scanning

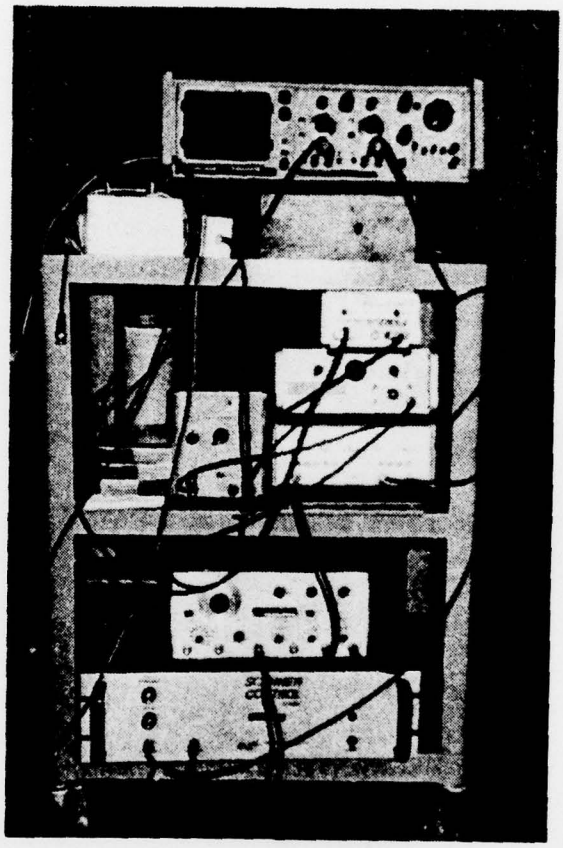

FIG. (43) Electronics

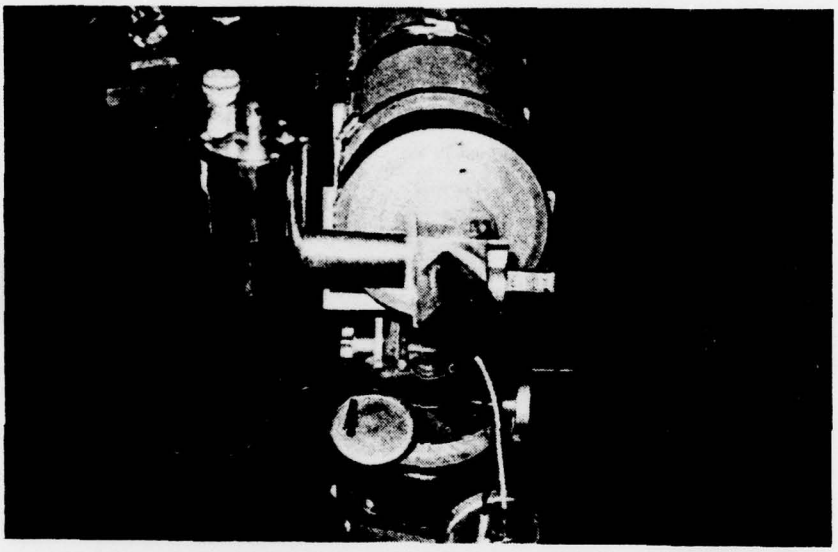

FIG. (44) Scanning Mirrors

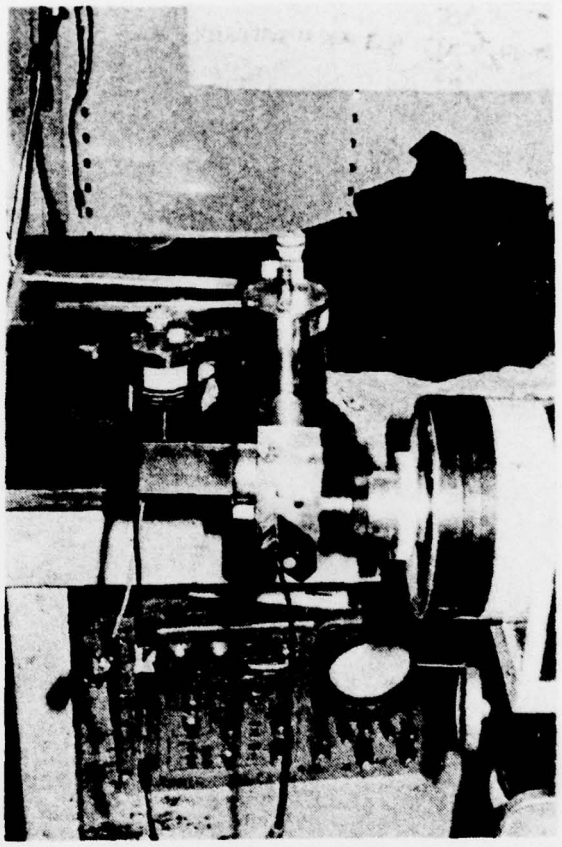

FIG. (45) Scan Mirrors and Detector in Dewar

APPENDIX C OPERATING INSTRUCTIONS

List of Equipment

Equipment Name	Symbol
WAVETECH MODEL 184 Function Generator	FG
GENERAL SCANNING CCX101 Scanner Control	SC
HEWLETT PACKARD 467A Power Amplifier	PA1 PA3
INTERSTATE ELECTRONICS CORP. P12 Pulse Generator	PG
PRINCETON APPLIED RESEARCH MODEL 113 Preamp	PAR
HEWLETT PACKARD 465A Amplifier	PA2
MONSANTO OS-226(P)/USM-368 Oscilloscope	OSCOPE

SIGNAL FLOW / SWITCH SETTINGS

FG
SWP OUT to (SC) External Input
PULSE OUT to (PG) Trig/Gate Input
50 Ω OUT to (PA1) INPUT

FREQ X1 Set 5 on dial
SYMMETRY Full CW
WAVEFORM
AMPLITUDE -20db, adjust fine as required

SC
POSITION (on back) to Mirror
DRIVE (on back) to Mirror
POSITION OUTPUT to (OSCOPE) Channel 2

Adjust OFFSET AND ATTENUATION as required

PA1
OUTPUT Connect both grounds
OUTPUT to (OSCOPE) Channel 1
OUTPUT (on back) to Mirror (slow)

AMPLIFIER X10

PAR
A/B from appropriate detector
OUTPUT to (PA2) Input

LF ROLL OFF - DC
HF ROLL OFF - 300K
Adjust GAIN as required
Set for AC operation

PA2
OUTPUT to(OSCOPE) Z input (on back) T connection

GAIN - 40db

PG
POSITIVE to (PA3) Input

Set voltage at 10 volts
Adjust delay and pulse width to blank flyback
Set for single pulse

PA3
OUT to Impedence box and then to Z input on (OSCOPE)

VOLT X2

OSCOPE
Both channels set for DC
Channel 1 .5 mV/DIV
Channel 2 20 mV/DIV
Adjust fine gains till picture is proper size
HORIZ DISPLAY - XY

INSTRUCTIONS

1. Adjust the function generator frequency and sweep controls until the desired raster is produced. Use the attenuation control on the scanner drive control to help with sweep size.

2. Adjust the pulse generator prior to imaging by blanking the sawtooth of the slow scan displayed on the oscilloscope.

3. Adjust the detector power supplies/bias circuits as required

4. Signal gain should normally be controlled only at the PAR 113, leave the HP465A at 40db.

5. Insure the diode box is connected correctly. Reverse connecting will cause signal loss.

6. Adjust oscilloscope controls to produce the correct size picture. The time base is not used for imaging.

7. During normal viewing, the oscilloscope INTENSITY control should be set as low as possible. This helps prevent raster perception. Focus the oscilloscope beam as fine as possible.

BIBLIOGRAPHY

1. Lloyd, J.M., Thermal Imaging Systems, Plemun Press, 1975.

2. Engstrom, E.W., "A Study of Television Image Characteristics," Part 1: Proc. IRE, p. 1631-1651, December 1933; Part 2: Proc. IRE, p. 295-310, April 1935.

3. Borg, S.B., "Thermal Imaging with Real Time Picture Presentation," Applied Optics, v. 7, No. 9, September 1968.

4. Edgar, R.F., "Some Design Considerations for Infrared Image Scanning Systems," Infrared Physics, v. 8, p. 183-187, 1968.

5. Hecht, E. and Zajac, A., Optics, Addison-Wesley, December 1968.

6. Hudson, R.D., Infrared System Engineering, Wiley, 1969.

7. Handbook of Military Infrared Technology, Office of Naval Research, Dept. of the Navy, 1965.

8. Electro-Optics Handbook, Technical Series EOH-11, RCA, 1974.

9. Williams, C.S., "Limitations on Optical Systems for Images of Many Discrete Elements of Area," Applied Optics, v. 6, No. 8, August 1967.

INITIAL DISTRIBUTION LIST

		No. Copies
1.	Defense Documentation Center Cameron Station Alexandria, Virginia 22314	2
2.	Library, Code 0142 Naval Postgraduate School Monterey, California 93940	2
3.	Department Chairman, Code 61 Department of Physics and Chemistry Naval Postgraduate School Monterey, California 93940	2
4.	Professor E. C. Crittenden Jr., Code 61ct Department of Physics and Chemistry Naval Postgraduate School Monterey, California 93940	2
5.	Professor A. Cooper, Code 61cr Department of Physics and Chemistry Naval Postgraduate School Monterey, California 93940	2
6.	LT James Powell Gruber, USN 2781 Avati Drive Columbus, Ohio 43207	2